Power Studies

AAEC/E79
NPCC/FEWP/P763
Tokai Mura TRCWP/P31

AUSTRALIAN ATOMIC ENERGY COMMISSION

RESEARCH ESTABLISHMENT

LUCAS HEIGHTS

IRRADIATION OF URANIUM METAL TUBES AND RODS IN A 4V HOLE IN HIFAR

by

B. S. HICKMAN

R. SMITH

R. J. HILDITCH

W. L. MERCER *

* G.E.C.-Simon Carves Atomic Energy Division, Erith, U.K.

Issued Sydney, October 1961

PREFACE

This report covers all aspects of the irradiation and post-irradiation examination of the specimens in the first test of metallic C.E.G.B. uranium in the HIFAR materials testing reactor. A preliminary report (NPCC/FEWP/P.667) issued in February, 1961, gave the results of the initial measurements and visual inspection of the specimens. The earlier report divided the specimens into three main groups into which they appeared to fall conveniently at the time. Further detailed examination, including a large amount of metallographic study, has suggested that it is better to divide the specimens into four groups with groups I and II including all results of direct application to power reactor fuel element operation. Certain sections of the present report repeat some of the information already given in the preliminary report.

CONFIDENTIAL

AUSTRALIAN ATOMIC ENERGY COMMISSION
RESEARCH ESTABLISHMENT
LUCAS HEIGHTS

IRRADIATION OF URANIUM METAL TUBES AND RODS IN A 4V HOLE IN HIFAR

by

B. S. HICKMAN
R. SMITH
R. J. HILDITCH
W. L. MERCER *

ABSTRACT

This is the final report on the first HIFAR hollow and solid fuel rod irradiation test carried out under contract to the U.K.A.E.A. (Irradiation Office Experiment No. 76).

* G.E.C. Simon Carves Atomic Energy Division, Erith, U.K.

CONTENTS

TABLES

continued

CONTENTS (continued)

FIGURES

1. INTRODUCTION

The first rig containing metallic uranium to be irradiated in the reactor HIFAR was successfully discharged from the reactor at the end of August, 1960. This rig contained seven pairs of test specimens of enriched uranium, the composition of which approximated to the PIPPA specification. Each pair consisted of a solid rod and a hollow rod, the latter with a sealed–off central cavity. The initial proposals for the test were outlined by Mercer and Slattery (1). The main purpose was to compare the irradiation stability of the two geometric forms of fuel under nominally identical conditions at temperatures of the order of 500 °C to a burn–up of about 3000 MWd/t. However the test has also provided useful general information on the behaviour of uranium under irradiation. This can be compared with existing data and has direct application to the U.K. civil reactor programme.

Early irradiation experiments on uranium carried out in the U.K. resulted in very large volume increases, but a large number of experiments over the last two years at A.E.R.E. Harwell have indicated that swelling is generally less than 10 per cent. at a burn–up of 4,000 MWd/t (2,3). The lower volume increases in these compared with the earlier experiments could be attributed to a number of factors, but is probably due to the use of larger specimens and to better temperature control in the later experiments. The most recent experiments were mostly carried out in the temperature range 400 – 650 °C to fuel burn–ups in the range 1000 – 4000 MWd/t. The results have a wide scatter, but in general they show that swelling is proportional to burn–up, and that the irradiation temperature is not an important variable in the range studied; however there is some indication that the swelling may be higher at the lower temperatures. Fuel rating also may be an important factor affecting swelling as some of the most highly rated specimens (i.e. operating at about 180 MW/t) showed only 2 per cent. volume increase at 4000 MWd/t burn–up, whereas most of the lower rated specimens (in the range 10 – 25 MW/t) showed two to three times this amount of swelling at lower burn–ups. Measurements made on Calder bars after irradiation (at a rating of about 1 MW/t) have, on extrapolation from a burn–up of about 2000 MWd/t, indicated amounts of swelling similar to the lower rated Harwell specimens (4). This suggests that there is no important effect of rating in the range 1 – 25 MW/t, but no account is taken of possible effects due to the difference in size of the irradiated rods.

The main uncertainties in the swelling behaviour of uranium under irradiation appear to be the effects of specimen size, fuel rating, thermal cycling, and the effect of temperature around 400 °C. The test described in this report may help to resolve some of these uncertainties. The test specimens were two or three times as large as the majority of the Harwell specimens, the fuel rating was in the lower range of the Harwell specimens, and, although no special attempts were made to control fuel temperatures during irradiation, the temperature fluctuations suffered by the majority of the test specimens were not excessive.

Little or no information is available on the relative stabilities of the solid and hollow rod forms of uranium fuel. American workers have reported "external geometric stabilisation" of U/1.6 wt.% Zr alloy fuel rods at elevated temperatures by the provision of a central axial cavity (5). Also a hollow rod 1.3 inch outer diameter showed good overall stability with all swelling inwards after a burn–up of only 1000 MWd/t, at a fuel surface temperature of 480 °C (6). However as very high temperature gradients were established in these specimens during the tests (the centre temperature approached 1000 °C) the results obtained are of little or no value in helping to assess the probable distortion of a Magnox–canned hollow–rod fuel element operating under U.K. power–reactor conditions.

The present test was initiated by G.E.C. in connection with the Tokai-Mura reactor project and was later made the subject of U.K.A.E.A. contracts. Specimens were fabricated by the Springfields Laboratory of the U.K.A.E.A. The irradiation rig was designed and assembled by the A.A.E.C. at their research establishment at Lucas Heights, and all post irradiation examination was carried out in the high activity handling cells at Lucas Heights. Out-of-pile control tests on an identical series of specimens were also carried out by the A.A.E.C. This report covers all aspects of the test excluding specimen fabrication. A preliminary report covering the initial stages of the post irradiation examination has already been issued (7).

2. EXPERIMENTAL TECHNIQUES

2.1 Test Specimens

The uranium specimens were manufactured in the enriched materials laboratory at Springfields from PIPPA specification uranium. Full details of the fabrication of the specimens have been given by Harris (8). Both types of specimen were cast as rods, heat treated using salt baths to yield a fine grain size, and machined to required dimensions. The hollow specimens were bored out from one end leaving a solid base, and a special welding technique was developed to seal off the central cavity with a thin zirconium end plug (9). A second beta-quench alpha-anneal treatment was given to these specimens to refine the coarse grain structure produced by welding.

The final nominal dimensions of the test specimens are shown in Figure 1. The analyses of the eight casts from which the fourteen in-pile and fourteen out-of-pile specimens were manufactured are given in Table I. All casts had compositions within the normal PIPPA range but the aluminium contents were higher than usual in PIPPA production metal; the solid specimens averaged 1380 p.p.m. and the hollow specimens 1260 p.p.m. compared with the usual PIPPA values of 550 – 750 p.p.m. The iron content was perhaps slightly high at 300 – 400 p.p.m. compared with 250 – 300 p.p.m. in PIPPA metal. The carbon content of the solid rods (900 – 950 p.p.m.) was significantly higher than that of the hollow rods (600 – 650 p.p.m.).

Metallographic examination of samples taken from each cast and heat treated with the irradiation samples showed a uniform fine grain size (Figure 23), and a normal distribution of U(CNO) inclusions and U-Al eutectoid structure.

Dimensions of all specimens were measured at Springfields and checked by the A.A.E.C. Densities were measured at Springfields by a water immersion method.

2.2 Irradiation Rig

The test was carried out in a four inch vertical hole (the 4V-2 hole) in HIFAR, a heavy water moderated and cooled test reactor practically identical to the DIDO reactor at Harwell. A standard A.A.E.C. 4V fuel rig (10) directly cooled by the heavy water was used for the test.

A general arrangement of the rig is shown in Figure 2. The rig consisted of two side-by-side aluminium tubes which dipped into the reactor heavy water and were protected by a perforated outer aluminium tube. Seven test specimens, double canned in stainless steel, were loaded into each of these tubes. A schematic cross section of one of these tubes showing the arrangement of the inner and outer specimen cans and the aluminium former into which the latter fitted, is shown in Figure 3. The outer stainless steel can was a push fit in the aluminium former which in turn was a push fit in the outer aluminium containing tube.

The width of the helium-filled gas gap between the two cans was chosen so that nuclear heating would raise the temperature of the inner can to the desired value during operation. The heat outputs of each specimen were calculated using flux data for a simulated 4V rig obtained during the low power operation of HIFAR (11); flux depression in the specimens was calculated by the empirical method due to Lewis (12). Individual heat transfer calculations to arrive at the gas gap dimensions were made for each can assuming only conduction and radiation losses across the gas gap (i.e. neglecting convection losses) and using temperature distribution data obtained in tests on a prototype out-of-pile rig. Mineral-insulated, stainless-steel-sheathed thermocouples were fitted into thermocouple pockets in each end of the specimen cans. The thermocouple pockets also served to position the inner can.

Each uranium specimen sat loosely in a zirconium cup designed so that contact between uranium and stainless steel was avoided during operation, and yet space was available for a considerable amount of fuel swelling. Cobalt thermal flux monitors in the form of 5 mg of cobalt wire, cemented into an alumina tube, were sealed in the space between the two stainless cans. The whole assembly was attached to a shield plug provided with service tubes and purge lines (to purge the space between the outer can and the aluminium containing tube). Thermocouples were connected to compensating leads at the top of the plug and the temperatures of all the specimens were recorded on multipoint potentiometric instruments.

The specimen positions were designated by a letter (A or B) indicating the stringer and were numbered consecutively from the top down. For convenience the specimens will be referred to by their position in the rig i.e. A-2, A-3 etc. Positions A-1 and B-1 were left vacant in this rig. For reference purposes, the positions, types, U.K.A.E.A. and A.A.E.C. specimen numbers, and design operating temperatures are given in Table II together with the specimen numbers of the corresponding out-of-pile control samples.

2.3 Rig Assembly

The inner cans were filled with high-purity double-distilled sodium in a pure helium atmosphere in a dry box; the sodium level was carefully adjusted and the end cap was welded in position under a helium pressure of one atmosphere without removing the cans from the dry box. After leak testing, which involved heating the specimen cans at 400 °C for 48 hours, the cans were radiographed to check the sodium level. The inner cans were then loaded into the outer cans, and welding carried out under one atmosphere pressure of helium in the dry box. Finally the cans were fitted with thermocouples, assembled into stringers, and loaded into the rig. All thermocouples were checked against a standard at 500 °C before use and shown to be within ±2 °C of the correct value. Great care was taken with the thermocouples during assembly and as a result no thermocouple failed during the whole period of operation.

2.4 Operation of Rig

2.4.1 First Approach to Full Power

Due to uncertainties in the heat transfer calculations and flux data it was expected that actual operating temperatures could be up to 100 °C different from the design temperatures. Hence to ensure that at least some specimens were close to the desired temperature of 500 °C, the operating temperatures were designed to span this temperature; the design temperatures for the seven pairs of specimens were 410, 440, 470, 500, 530, 560, and 590 °C respectively. (See Table II). At the first approach to power with the rig loaded, the reactor power was levelled-off at 9 MW and the indicated temperatures, except for position B-6, were all below but within 15 per cent. of the predicted values. The indicated temperatures for specimen B-6 were 600 °C on the upper thermocouple and 660 °C on the lower thermocouple, well above the predicted value of 530 °C. It appeared therefore that all specimens except B-6 would operate very close to their intended conditions at the full reactor power of 10 MW.

2.4.2 Period of Fluctuating Temperature Operation

On starting-up the reactor a second time, considerable variations were obtained from the initial temperatures and some specimen temperatures fluctuated for about 700 hours after commencement of the test; during this period there appeared to be little correlation between reactor power and specimen temperatures. The temperature histories of the specimens as indicated by the lower thermocouples are shown in Figures 4 and 5 for this period of operation. Temperatures were taken from the instrument recorder charts but small variations of up to $\pm 5^{\circ}C$ have not been shown. Cycles to low temperatures which occurred on reactor shut-downs have been shown only for long shut-downs. Unscheduled short shut-downs (generally of 1 – 2 hours duration) and the longer shut-downs are indicated by the arrows on the top of the graphs. The reactor power level at different stages of operation is also shown at the top of the figures.

As can be seen from the figures, specimens in stringer B showed much greater variations than those in stringer A. In particular, specimens B-3, B-4, and B-5 showed gradually increasing temperatures and specimen B-6 maintained a high temperature. All these specimens almost certainly spent some time in the β-phase during this period. Specimens B-5 and B-7 cycled continuously over the period; the upper thermocouples followed much the same pattern as the lower thermocouples indicating that the observations were genuine.

In an attempt to correct this situation the carbon dioxide atmosphere in the rig was replaced with helium during the shut-down which occurred after 550 hours of operation. The samples by this time had received approximately 8 per cent. of their total dose. At the subsequent start-up, most temperatures in stringer B again reached high values. Specimens B-4 and B-6 probably entered the γ-phase and B-3 and B-8 entered the β-phase. However the temperature fell rapidly over the first few hours of operation and finally returned to close to the desired values enabling the reactor power to be raised to 10 MW.

The temperatures of specimens in stringer A were relatively constant for the whole of this initial period of operation.

A satisfactory explanation for the abnormal behaviour of the specimens in stringer B during this period of operation cannot be put forward. Other rigs of identical design have not shown this effect at all. The most obvious explanation would be that a small leak in the outer stainless steel cans allowed some of the helium in the gas gap to be displaced by carbon dioxide, thereby reducing the thermal conductivity of the gas. However the cans were all tested after irradiation and no leaks could be detected. Also it is very hard to see why this effect should be limited to one stringer. Possibly it was associated with changes in the conductance between either the outer can and the aluminium former, or the aluminium former and the outer containing tube.

2.4.3 Period of Steady Operation

As mentioned above, the temperatures of the specimens in stringer B settled down to steady values after about 700 hours had elapsed and the temperatures of both stringers remained relatively constant for the rest of the period of operation. The temperature history of the specimens for this period of operation as indicated by the lower thermocouples is shown in Figures 6 and 7. These charts were plotted on the same basis as Figures 4 and 5 except that the eight-hourly logs of the sample temperatures were used. (See Section 2.4.2). It can be seen that even during this period of operation the temperatures of stringer A specimens were generally more stable than those of stringer B specimens. Specimen B-5 in particular continued thermal cycling at intervals throughout the test.

2.4.4 Thermal Cycling

Apart from the initial behaviour of some samples in stringer B and the continued cycling of specimen B-5, it is considered that the thermal cycles which occurred at reactor shut-downs would swamp all other cycling effects. A total of 31 shut-downs or trips occurred during the six month period of the test. The shut downs were far more frequent during the initial stages of the test as 21 trips or shut-downs occurred during the first 30 per cent. of the total fuel burn-up and the last 10 occurred during the final 70 per cent. At shut-downs the specimen temperatures fell from the operating temperature to the shut-down temperature of 40 °C at about 100 - 200 °C per minute. Reactor start-up was also fairly rapid, operating temperatures being reached 10 - 15 minutes from divergence. Apart from cycles at shut-downs, other temperature changes were generally very slow drifts and are not thought to have affected the behaviour of the specimens (except of course B-5).

2.4.5 Relationship between Indicated and Actual Temperatures

It must be emphasised that all the temperatures plotted in Figures 4 to 7 are those indicated by the lower thermocouples; these are lower than the true specimen temperatures.

It has been suggested recently (2) that when specimens are immersed in liquid sodium, large temperature differences may exist between the bulk sodium and the uranium surface as a result of sodium film-boiling. However, this suggestion applies to much more highly rated specimens than the present ones and need not be considered further. Nevertheless small temperature differences must be present which cannot be accurately evaluated by calculation. Only a special in-pile test or a simulation test using an electrically heated specimen will resolve this particular problem. Clough (13) examined the problem in the light of recent A.E.R.E. experience and concluded that a longitudinal temperature gradient of 5-10 °C/cm exists along the specimens during operation (hotter at the top) and that the surface temperature at the bottom may have been 10 - 15 °C hotter than the thermocouple temperature.

It is important also to consider the centre temperature achieved during operation. The original design calculations (1) indicated that the highest-rated solid and hollow specimens would operate with surface to centre temperature differences of 18 °C and 26 °C respectively. However, during most of the test (at 10 MW reactor power) the ratings were higher than anticipated giving estimated values of 21 °C and 30 °C respectively. Irradiation may have had a further effect by decreasing the thermal conductivity, thereby raising the centre temperatures of the test specimens. Recent measurements on irradiated Calder uranium have indicated that the thermal conductivity of the metal decreases rapidly during early irradiation and then more slowly to give a total decrease of about 20 per cent. at a burn-up of 3000 MWd/t. Assuming that these changes can be applied to the HIFAR specimens, and ignoring the deleterious effects of cracking, the surface to centre differences towards the end of the test would be 27 °C and 39 °C for the highest-rated hollow and solid rod specimens respectively.

It appears therefore that the additive effect of the temperature difference between the thermocouple and the specimen surface (assuming a mean value of 20 °C) and the temperature difference between the surface and the centre of the specimen will result in actual specimen centre temperatures of 50 - 60 °C above the indicated temperatures on the lower thermocouples. However metallographic examination of the specimens has indicated that the difference may be even greater than this as two specimens which had maximum indicated temperatures of 570 °C and 590 °C on the lower thermocouples showed definite evidence of β-phase operation. This is discussed more fully in Section 4.1.

The upper thermocouple was intended to be purely a safeguard thermocouple should the lower thermocouple fail. Since the thermocouple pocket was only just dipping into the sodium, the reading of this upper thermocouple is not thought to have been very reliable. From Clough's analysis one would expect the upper thermocouple to read higher than the lower; in some instances this did occur indicating that for those cans the upper pocket was sufficiently immersed to give a more correct reading. However, in the majority of cases the upper thermocouple read about the same or less than the lower.

2.4.6 Summary of Operating History

The temperatures indicated by the various thermocouples during operation are summarised in Table III which shows the desired temperatures, the maximum temperatures indicated during the initial period of fluctuating temperatures, the temperature range, and an estimated mean temperature during the steady period of operation. It can be seen that specimens B-3, B-4, B-5, B-6, and B-8 almost certainly underwent some β-phase operation during the initial period of the test. Subsequently all specimen temperatures settled down to fairly steady operation somewhere in the range 360 - 560 °C. During this period stringer A specimens were more stable showing temperature drifts of up to ±20 °C whereas some stringer B specimens showed drifts of up to ±50 °C. It must be emphasised again that these temperatures are not true specimen temperatures but those indicated by the thermocouples.

2.5 Post Irradiation Examination Procedure

Dismantling of the rig and examination of the test specimens were carried out in concrete shielding cells at Lucas Heights. The rig was dismantled by cutting and the outer specimen cans extracted. Some of these cans were subjected to a silicone oil leak test but no leaks were detected. The outer cans were than removed by milling and the cobalt monitors extracted. Visual examination of the inner cans through the cell windows showed no evidence of distortion or sodium leakage. The gas above the sodium in the inner cans was sampled by piercing the cans in an evacuated system of known volume; the pressure rise in the system was measured and the composition of gas samples was determined by mass spectrometry. The inner can was heated to 150 °C during piercing to melt the sodium and release any entrapped gas. The top of each inner can was then milled off, the sodium melted and poured out, and the specimens extracted. Subsequent procedures depended on the type of specimen:-

Rod Specimens

(i) Final traces of sodium were removed by immersion first in alcohol and then in water.

(ii) Macro-examination and photography were carried out using a Bausch and Lomb stereo-binocular microscope.

(iii) Detailed dimensional checks were made at many positions using a Bausch and Lomb optical gauge.

(iv) Densities were measured by weighing in air and then in water, care being taken during the latter process to remove entrapped bubbles by vacuum impregnation.

(v) Axial and longitudinal sections for metallography were then cut with a diamond slitting wheel. The details of these sections are shown in Figure 8.

Tube Specimens

(i) The specimens were washed thoroughly in alcohol and then weighed in air.

(ii) Macro-examination and photography were carried out.

(iii) Detailed dimensional measurements of all specimens were made.

(iv) Those specimens showing no increase of weight and no evidence of cracking (i.e. specimens A2 and A4 in which there was no ingress of sodium into the inner cavity) were washed thoroughly in water and their bulk densities determined by weighing in air and then in water after vacuum impregnation. These specimens were then placed in the gas sampling rig and samples of the gas in the inner cavity taken by drilling through the zirconium end-plug.

(v) The welded end of each specimen was then removed by slitting and the base examined macroscopically. Any sodium present in the tube was dissolved out and the internal diameter of the tube was determined approximately by means of plug gauges.

(vi) The uranium metal density was then determined by weighing the sectioned tube in air and then in water.

(vii) Further sectioning for metallography as shown in Figure 8 was then carried out.

Specimens of both rods and tubes were mounted for metallography in Araldite casting resin. Sections B and C of the rods and tubes (Figure 8) were mounted to give transverse and longitudinal sections, and section D of the tubes was mounted longitudinally to give a cross section of the weld. The most satisfactory method for preparation of the metallographic specimens was found to be:

(i) Grind on 120, 220, 320, 400, and 600 grade silicon-carbide papers on a Buehler automet machine modified for remote operation.

(ii) Polish on a Syntron vibratory polishing machine for about two hours using a nylon cloth and a medium grade alumina polishing compound.

(iii) Attack-polish on a Syntron vibratory polishing machine using a nylon cloth, a medium grade alumina, and a chromic-acetic acid solution until a satisfactory polish was achieved (generally 2 - 4 hours). The chromic acetic acid solution was made up from 50 parts of saturated chromium-trioxide solution, 100 parts of glacial acetic acid, and 100 parts of water.

Examination and photography of the polished specimens were carried out on a Reichert remote controlled metallograph.

Accurate burn-up determinations were made on halves of specimens A-6 (Section C) and B-6 (Section A). This was carried out by dissolution of the weighed sample and separation of the fission products by the method described by Farrell (14). The weighed samples were dissolved in boiling concentrated nitric acid. A preliminary separation of the uranium from the fission products was carried out using solvent extraction by a 20% T.B.P. solution in kerosene.

Further decontamination was carried out by ion exchange in a silica gel column followed by a further solvent extraction stage. The final solution was analysed for U-235/U-238 and U-236/U-238 ratios using a mass spectrometer as described by Whittem (15). These ratios were compared with the ratios in an unirradiated control sample from the same cast and the total U-235 burn-up and U-235 fission burn-up calculated.

The activity of the cobalt monitors was estimated by comparison with standard Co-60 sources in a constant geometry gamma-spectrometer, using a collimator through the cell wall. The standards were calibrated by dissolution and $4\pi\beta$ counting, and by a Victoreen electrometer.

2.6 Out-of-Pile Control Tests

A duplicate of each irradiation specimen (see Table II) was canned in sodium in a stainless steel can in the same manner as the irradiation specimens and subjected to a similar heat treatment. The heat treatment was based on the thermocouple readings from the corresponding irradiation specimen but did not follow minor variations in irradiation temperature. Owing to failure of the furnace controllers three control specimens were subjected to operation at temperatures in excess of 1000 °C for short periods. Two of these were lost entirely due to can failure and oxidation.

3. RESULTS

3.1 Burn-Up Determination

The estimated burn-ups of the specimens as determined by the various methods are given in Table IV. The figures are quoted as percentage burn-up of the uranium as this is thought to be less ambiguous than MWd/t. An approximate conversion from per cent. burn-up to MWd/t is that 1 per cent. burn-up = 9650 MWd/t. The burn-up figures quoted in the four columns were obtained by the following methods:-

Method 1 – Calculation from the latest HIFAR flux data (based on measurements carried out at low power) assuming that the mean flux in the specimen was 72 per cent. of the flux in the rig in the absence of the specimen.

Method 2 – From fluxes estimated from the gamma-spectrometry of the cobalt monitors using $4\pi\beta$ counting as the standardisation technique. Again it was assumed that the mean flux in the specimens was 72 per cent. of the flux at the cobalt monitor position.

Method 3 – As for column 2 but using a Victoreen electrometer as the standardisation technique.

Method 4 – From the mass spectrometry of uranium chemically separated from the specimen.

The results from the various methods are in good agreement and they show a peak burn-up of 0.36 per cent. to 0.37 per cent. in the specimens in the centre of the rig falling off to 0.28 per cent. to 0.31 per cent. in the specimens at extremities.

3.2 Out-of-Pile Controls

Macro-examination of the out-of-pile control specimens showed no evidence of distortion or cracking and the densities and dimensions showed no changes as a result of heat treatment. Micro-examination showed that specimens which had not been subjected to β-phase operation had an identical microstructure to the as-received specimens (Figures 23, 24). Specimens which were subjected to β-phase operation showed a considerably increased grain size (Figure 25) but no evidence of cracking.

3.3 Visual Examination of Irradiated Specimens

The results of the visual examination of the specimens are summarised in Table V. This examination showed that the specimens could be divided into four groups as follows:

Group I – Specimens which showed very little change as a result of irradiation with little or no cracking and no change in geometrical shape. Two hollow and two solid rod specimens, A–4, A–5, A–6, and A–7, fell into this group.

Group II – Specimens which showed major changes in shape with extensive surface wrinkling but with no evidence of cracking. One hollow and two solid rods fell in this group, namely A–2, A–3, and B–2.

Group III – Specimens which exhibited no significant overall change of shape but which showed extensive surface cracking and roughening. Five specimens came into this group, three hollow and two solid rods, namely A–8, B–5, B–6, B–7, and B–8.

Group IV – Specimens which showed major changes of shape and extensive cracking. One solid and one hollow rod fell into this group, namely, B–3 and B–4.

These groups of specimens are considered in detail below.

NOTE The magnification shown on Figures 9 – 22 included with this report should be multiplied by 1.5.

3.3.1 Group I – Specimens Showing Little Change, A–4, A–5, A–6, A–7

The specimens in this group appeared very similar to unirradiated specimens. Solid rod A–7, the most stable specimen in the test, showed no trace of damage (Figure 9). Hollow rod A–6 was similar, but slight circumferential cracking could be seen in the uranium outside the end plug weld pool and slight cracking was observed on the lower end of the specimen (Figure 10). There was also slight evidence of surface roughening. Specimens A–5 and A–4 remained true right cylinders with no sign of cracking but slight surface roughening was detected on both (Figures 11 and 12).

It can be seen from the photographs that surface roughening (or wrinkling) was greatest on A–4, and was not visible on A–7; these specimens were irradiated at the lowest and highest temperatures respectively of those in this group. Specimens A–5 and A–6 which were irradiated at intermediate temperatures had an intermediate degree of wrinkling. However none of the wrinkling effects were severe. The hardness indentations made on the ends of specimens before irradiation were still clearly visible on all specimens after irradiation. Also the machining marks were still distinct and relatively undistorted, except in the case of A–4 where they were partly obliterated on the outer regions of the plain end.

3.3.2 Group II – Specimens Showing Severe Surface Roughening, A–2, B–2, A–3

The three specimens in this group are shown in Figures 13, 14, and 15. In each specimen there was severe wrinkling but again the severity was temperature dependent as it was greater in A–2 and B–2 than in A–3 which was irradiated at a higher temperature. Associated with the wrinkling and following the same pattern with temperature, there was an overall change of shape of the specimens – a bulging or increase in diameter of the ends of the cylinders together with a dishing of the ends (apart from the welded end of the hollow–rod specimen).

No cracking was observed in this group of specimens except for slight circumferential cracking around the weld pool in A-2 similar to that observed in Group I specimen A-6.

3.3.3 Group III - Specimens Showing Extensive Cracking, A-8, B-5, B-6, B-7, and B-8

All five specimens in this group retained their shape as right cylinders but they all showed cracks, usually extensive. There was no evidence of surface roughening of the type observed in specimens from Groups I and II. The specimens are shown in Figures 16 - 20, approximately in the order of increasing severity of cracking (i.e. A-8, B-8, B-7, B-6, and B-5). There were no signs of cracks on the plain end of specimen A-8 but a network of fine cracks could be seen on the walls, more so towards the welded end. Similar networks of cracks were visible on all uranium surfaces of specimens B-7, B-6, and B-5, varying from fine cracks in B-7 to some coarse cracks in B-5. Specimen B-8 did not show a network of cracks but rather a few isolated short wide cracks (Figure 17).

Cracking was quite deep in both solid and hollow specimens and, in the hollow specimens at least, the networks of cracks were continuous throughout the section. This was confirmed later when it was found that all the hollow rod specimens in this group had filled with sodium. The white deposit which can be seen in Figure 18 is a sodium-alcohol reaction product which came out of the cracks during examination; presumably this was forced from the cracks by chemical reaction in the central cavity.

The three hollow rod specimens showed cracking around the outside of the weld pool similar to that observed in Group I and II specimens.

3.3.4 Group IV - Specimens Showing Cracking and Major Geometric Distortion

These specimens are shown in Figures 21 and 22. Both specimens showed considerably worse distortion at the lower end than the upper end. Specimen B-4 in particular had distorted so much at the lower end that it jammed in the zirconium bucket and had to be sectioned before it could be removed, whereas the upper end showed no cracking at all and comparatively minor surface roughening. In both cases the lower ends of the specimen were badly cracked, with considerable displacement of metal on either side of the cracks to give large steps on the surface. Apart from circumferential cracking similar to that noticed around the welds in most specimens, the welded end of B-3 was not unduly affected. An unusual effect in B-3 was the apparent partial collapse of the wall of the specimen (Figure 20).

Macro-examination of the bore of all tube specimens after sectioning showed no effects not already noted in the examination of the exterior of the specimens. As expected from the weight gains, hollow specimens B-3, B-5, B-7, A-6, and A-8 all showed evidence of sodium penetration through cracks to the central cavity.

3.4 Dimensional and Density Changes

The changes in dimensions are listed in Table VI and changes in densities in Table VII. All density figures quoted for the tube specimens are the uranium metal density after sectioning, except for specimens A-2 and A-4 where both the bulk density and the uranium density are quoted. The changes in linear dimensions were determined by comparing post-irradiation values with values determined by the A.A.E.C. before canning. The changes in density were related to pre-irradiation values determined at Springfields during manufacture of the test specimens (8). The dimensions were measured to ±0.0002 inch and the densities to ±0.05 g/cm^3.

Distortion of specimens A–4 to A–8 and B–5 to B–8 was regular and the mean values were not very different from the measured maximum and minimum values obtained from measurements at different places on each specimen. Local deformation, namely end dishing and bulging, on the four specimens, A–2, B–2, A–3, and B–3, resulted in mean values which must be used with caution. For example, solid rod B–2 showed a mean length decrease of 0.1 per cent. which, as a result of end dishing, was associated with a maximum outer rim "growth" of 1.1 per cent. and a maximum core "shrinkage" of 2.9 per cent. No other specimen showed a length decrease, even when measured at the centre of the dish. Solid rod A–3 showed a growth of 0.3 per cent. at this position. For the hollow specimens it was only possible to repeat the pre–irradiation measurement taken at the centre of the zirconium end plug. No measurements were taken at the edge of the specimen. The estimate of the dishing of the plain end of A–2 was obtained by measuring with the welded end placed on the anvil of the optical gauge and it is probably not very accurate. Diameter measurements only are given for specimen B–4 because as mentioned earlier this specimen had to be sectioned in order to extract it from the zirconium cup. These measurements were taken only on the relatively sound upper end as no measurements could be made on the heavily distorted lower end. A rough measurement of the inside diameter of the tube specimens was made using plug gauges and the results are given in Table VI.

Swelling figures are given in Table VII, together with the changes in density. These figures have been calculated from the measured changes in density and they represent the change in volume of the metal in each specimen as a result of the irradiation. For the Group I specimens, A–7, A–6, A–5, and A–4, the swelling was small as the highest figure was 1.7 per cent.; for the Group II specimens, A–2, B–2, and B–3, which showed marked wrinkling, the swelling was greater, up to 8 per cent. in the case of A–2; for the Group III and IV specimens the swelling figures varied from 1.3 per cent. to 4.7 per cent.

The swelling figures given in Table VII may be compared with figures given in Table VI calculated from the mean changes in outer dimensions; these latter figures represent the overall volume increases of specimens as distinct from the volume increases of the metal. These two sets of figures would be the same if the uranium remained uncracked and undistorted after irradiation. This is almost true for the Group I specimens, and there is reasonable agreement between the two sets of figures. However in all other cases the overall volume increase calculated from dimensional change is appreciably greater than that calculated from the change in density. In the case of the specimens in Group III, this difference is to be expected because of the extensive macroscopic cracking in the metal which affects the outer dimensions but not the density measurements. In the case of the Group II specimens, the difference is not due to cracking but rather the roughening of the surface and macroscopic distortion. In the case of the Group IV specimens the difference arises from a combination of both cracking and distortion.

3.5 Gas Release

The available results of analysis of the gas above the sodium level in each can are shown in Table VIII. Results are not available for specimens A–2, B–2, A–3, B–6, and B–7. Also included in the table are the results of the analysis of the gas from the inside of tubes A–2 and A–4, the only tubes in which no cracking occurred. The high argon content (4 per cent.) of solid rod B–8 cannot be explained, but otherwise the argon figures are consistent with the results of the macro–examination. In the case of the tube specimens B–3, B–5, and A–8 in which there was extensive cracking, argon has been released from the bore into the sodium, whereas in specimens A–2 and A–6, which showed little or no cracking, there has been little or no leakage through the metal.

The percentages of the generated fission–product gases which were released into the cans are shown in Table IX. These were calculated using the method outlined by Barwood et al. (16).

The results show that in the Group I specimens which showed no distortion or cracking the gas release was low, being between 0.14 per cent. and 0.25 per cent. However in those specimens which showed extensive cracking and distortion (Groups III and IV), the gas release was usually higher. The highest figures were obtained for specimens A–8 (0.6 per cent.) and B–3 (1.1 per cent.).

3.6 Metallography

The results from metallographic examination of the specimens are summarised in Table X. Typical photographs of microstructures are shown in Figures 26 to 45. These have been reduced approximately 20 per cent. for reproduction. Specimens A–3 and A–5 were not examined as it was considered they would not show any features not observed in other specimens. For convenience the specimens are divided into the same four groups as were used for describing the results of the macro–examination. Apart from the welds, which will be considered later, the features observed in the specimens in these groups were as follows:–

Group I – A–7, A–6, A–4, Specimens showing little change (Figures 26, 27, 28)

In general the microstructures of specimens in this group were identical to those of the control specimens as they showed fine irregular–shaped grains with little evidence of twinning i.e. they showed no observable effects due to irradiation. However in specimens A–6 and A–4 this was not true of the complete specimens.

In hollow rod A–6 at the bottom end of the tube there was slight intergranular cracking, the grain shape was more regular, and there was a faint network of cavities not associated with grain boundaries, Figures 27 (b) (c) (d) (e).

In hollow rod A–4 the grains near the outer surfaces, particularly those near the junction between the base and the walls, showed a significantly higher density of twins than those grains in the interior of the specimen (Figure 28 d). This effect was not observed in specimens A–7 and A–6 which operated at significantly higher temperatures during the operating period. The density of twins appeared to be directly related to the intensity of wrinkling but there was no obvious relationship between individual wrinkles and either single grains or groups of grains.

Group II – A–2, B–2, Specimens showing wrinkling effects (Figures 29, 30)

Specimens A–2 and B–2 were similar and the main observations were as follows:–

(a) There was no evidence of any cracking or porosity.

(b) The grain–size was unchanged.

(c) Within the grains there was extensive complex twinning which was much more severe towards the outside of the specimens. Near the outside surface the twinning was so extensive that it was difficult to distinguish the grain structure. In hollow tube A–2, associated with the less severe twinning towards the bore, there was less evidence of wrinkling in the bore than on the outside surface.

(d) There was no obvious relationship between individual wrinkles on the surface and either individual grains or groups of grains of similar orientation.

(e) There was no metallographic evidence at magnifications up to X500, to account for the large swelling in these specimens.

Both of these specimens were difficult to prepare as they pitted readily during attack-polishing; also, it was difficult to obtain any contrast between the grains under polarised light.

Group III - A-8, B-7, B-6, B-5, B-8, Specimens showing extensive cracking (Figures 31 to 37)

The structures of the specimens in this group varied considerably from specimen to specimen. However in all cases the extensive cracking was associated with a coarse grain size produced by single or multiple temperature excursions into the β-phase field or higher.

Another common feature of these specimens, and in fact of all specimens which showed cracking, was the presence of significant amounts of uranium hydride. This was always closely associated with the cracks (Figure 32b) and since it is thought to have formed after irradiation during dissolution of the sodium, it will not be considered further.

One of the most interesting specimens in this group is A-8 (Figures 31 and 32). In this hollow specimen the structure at the bottom had not changed during irradiation and it was similar to the Group I specimens. However along the wall, there was clear evidence that at some stage during the test a temperature gradient existed which spanned the alpha-beta critical temperature. Figure 31c shows this effect and it can be seen that following the temperature excursion, the reverse transformation from beta to alpha uranium has occurred slowly in a temperature gradient to produce a region of columnar grains followed by large equi-axed grains further along the wall (Figures 31a and 32). In the coarse-grained regions produced by the temperature excursion into the β-phase field there was extensive intergranular cavitation and cracking together with some minor transgranular tears or cracks (Figure 32). Most of the intergranular cracks appeared to have formed by the joining together of series of grain-boundary holes. The origin of these holes will be discussed later but at this stage it is worth noting that they appear to be associated with grain-boundary sliding, as shown by the grain boundary displacement in Figure 32d, the relative distribution of holes along the sides and ends of the columnar grains in Figure 31b, and the distribution of the transgranular tears in Figure 32a.

A significant point of interest about specimen A-8 was that although part of the specimen must have risen to a temperature in the β-phase region, the maximum temperature recorded by the lower thermocouple was 570°C. In specimen B-7 also, the thermocouple records showed only α-phase operation whereas metallographic examination showed that the temperature must have risen into the β-phase region. Possible reasons for these discrepancies are discussed in Section 4.1.

The structure of specimen B-7 was very complex, and it varied considerably in different positions. At the bottom of the tube most of the section was extremely coarse grained with grains the same size as the thickness of the base except for a thin fine-grained region near the inner surface (Figures 34a, 34b, and 34c). Along the walls, the grain-size was finer but it varied considerably over small regions (Figures 33a and 33c).

The network of cracks was similar in character to that in specimen A-8 except that in general the cracks were not around the present grain boundaries but appeared to outline a grain structure which existed previously.

Specimen B-6 (Figure 35) was similar to the coarse grained part of specimen A-8. However again the network of cavities and cracks did not always outline the existing grains (Figure 35d).

Specimen B-5 (Figure 36) was very coarse-grained, and there were practically no cracks around the present grain-boundaries. Instead there was a coarse network of inter-granular cracks and cavities apparently outlining a previously existing coarse grain structure.

Specimen B-8 (Figure 37) was somewhat different from the other specimens in this group from the point of view of the shape of the grains. In this case the grains were also coarse but they were very irregular in shape with well defined sub-grains. Intergranular cracks and cavities followed the irregular grain boundaries but they were less extensive than in other specimens in the group. There were also some short well-separated transgranular cracks at the surface (Figure 37 e) together with transgranular tears in the interior (Figure 37 b).

Group IV - B-3, B-4, Specimens showing cracking and geometric distortion (Figures 38 and 39)

Both of the specimens in this group had had temperature excursions into the γ-phase region during the early period of operation. This was presumably the cause of a feature which was observed only in these specimens, namely, the presence of a fine precipitate preferentially orientated within the grains.

Specimen B-3 had an extremely coarse grain size with massive intergranular cavities and cracks. Associated with the cracks there were marked displacements at the surface.

The badly cracked end of specimen B-4 was not examined but presumably its structure would be similar to that of B-3. The upper end was completely sound with no evidence of cracking and only slight indications of surface irregularities (Figure 39). The grain size was medium.

Structure of the Welds

No detailed examination of the structure of the welds was attempted apart from examining the sectioned surfaces for evidence of cracking. Typical micro-photographs are shown in Figures 40 to 45. As may be seen from these figures the quality of the weld varied considerably from specimen to specimen and also from one side of a specimen to the other. In specimen A-6 there was a marked crack across the weld metal, but in all other cases the welds themselves were sound, and any cracking present was found only in the uranium in the Group III and IV specimens. Specimens which had been heated to temperatures in the β-phase region, and higher, showed thickened zones where interdiffusion between the zirconium and weld metal had occurred.

3.7 Summary of Results

In order to ease comparison of the various changes produced in the test specimens by irradiation, the principal results are summarised in Table XI. Again, to present a clearer picture the specimens have been divided into the four groups used for the description of the macro- and micro- examination.

4. DISCUSSION

4.1 Relationship between Indicated and Actual Specimen Temperatures

As mentioned in the description of the operating temperature of the specimens (Section 2.4), the specimen surface temperatures were certainly higher than the temperatures indicated by the lower thermocouple, and the calculations by Clough indicate that this difference would be about 20 °C for the highest rated specimens in this test. However the following facts are relevant to this point:

(i) Specimens A–8 and B–7, which had maximum indicated temperatures on the lower thermocouples of 570 °C and 590 °C respectively, entered the β–phase indicating that the error may have been as high as 100 °C at some stage.

(ii) The extent of the wrinkling in specimens A–2, B–2, and A–3 suggests that the steady operating temperatures of these samples could not have been more than 20 – 30 °C above the indicated temperatures or the wrinkling would not have been so severe.

It appears therefore that, whereas the estimate of 20 °C for the thermocouple error could be correct for steady operating conditions, transient conditions could have occurred which resulted in higher temperature–errors. It seems likely that this could happen during an approach to full power. During the period of the test the general procedure was to raise the reactor power from 1 MW to 9 MW in 2 MW steps, and then to 10 MW, allowing a few minutes at each step but making the changes in power in 10 – 20 seconds. Examination of the temperature records showed that the indicated specimen temperatures generally fell 10 – 15 °C in the first few minutes after reaching a given power level and often fell another few degrees over the next 1 – 2 hours. Evidently a peak in temperature occurred on first reaching full power. Taking into account the likely time lag between specimen temperature and thermocouple response and the fact that the temperatures are only recorded about once a minute it is quite probable that temperature transients of at least 50 °C above the steady operating value could be obtained. This would satisfactorily explain the β–phase operation of specimens B–7 and A–8.

The results also confirm Clough's suggestion that there is a temperature gradient up the specimen. The greater extent of the wrinkling at the lower ends of specimens A–2 and A–4, the greater distortion at the lower end of B–3, and the fact that only the upper half of A–8 suffered β–phase operation, all confirm this view.

4.2 Behaviour of Group I Specimens

One of the most striking results of the test was the virtually unchanged appearance of the Group I specimens. The swelling in all four of these specimens was very low (1.3 to 1.7 per cent.) and in fact it was very little greater than that predicted due to the incorporation into the structures of the extra atoms produced by the fission process. The stability of these specimens compared with that of Group II – IV specimens must be due to the fact that they did not suffer β–phase operation and operated for the majority of the test above the wrinkling temperature range. The only anomalous result in these specimens was the fine cracking in the lower end of specimen A–6 which was apparently associated with a somewhat different grain structure. No explanation can be offered for this result.

Apart from the cracking in A–6, these specimens showed no deleterious effects resulting from the 31 major thermal cycles from operating temperature to 40 °C, and the slow temperature drifts of up to ±20 °C.

4.3 Behaviour of Group II Specimens

The extensive wrinkling in Group II specimens is obviously due to the fact that they operated at temperatures low enough for them to be in the irradiation–growth temperature range.

The large volume increases in these specimens compared with those irradiated at higher temperatures must again be associated with the anisotropic growth process. Pugh (2) reports that similar large volume changes have been observed at Harwell in specimens irradiated in the growth temperature range. The mechanism of these volume changes is not clear. They could be due to grain boundary cavitation resulting from grain boundary sliding but no evidence was obtained for this from the optical metallography. Electron microscopy would be required to elucidate this point.

The two solid rods in this group (B-2 and A-3) suffered larger mean changes in diameter than in length and a similar effect could have occurred in the hollow rod A-2, but would not have been observed owing to the method of measurement.

End-dishing and bulging at the ends of the circumferential surfaces were observed in all specimens in this group. Presumably this distortion must have arisen as a result of irradiation-growth; the fact that the density of twinning decreased on moving from the outer rim to the centre suggests that more irradiation-growth has occurred in the outer rim. However, with the information available, it is difficult to see how distortion of this type can be produced. If there were some preferred-orientation texture present, the macroscopic distortion could be explained as a result of higher burn-up and lower temperatures in the outer rim. Alternatively it could be explained if there were variations in the degree of preferred orientation or type of texture across the bar. Recent measurements on production Calder bars have indicated the presence of a texture which varies across the diameter, and when these bars were irradiated in the irradiation-growth temperature range it was found that end-dishing and overall bar growth or shrinkage occurred depending on the temperature and the temperature gradient from surface to centre of the bar.

4.4 Behaviour of Group III and Group IV Specimens

The Group III and Group IV specimens were all heated into the β-phase or γ-phase during the early stages of the test, thereby producing a very coarse grain size. Thus the results from these specimens are of little application to reactor fuel element performance except to emphasise the importance of a fine grain size even at higher operating temperatures out of the growth and wrinkling range. Detailed speculation on the behaviour of these specimens is not warranted, particularly in view of their complicated temperature histories, but it is interesting to note that most of the cracking outlined the existing boundaries of the coarse grains or a previously-existing grain boundary network, and that in general the cracks appeared to be preceded by void formation. Two processes could have occurred to produce these effects, namely grain-boundary sweeping of fission-product gases and grain-boundary sliding. The first of these would occur during phase changes, when there is a tendency for the fission product gases to be swept by the advancing interfaces and concentrated in the new grain boundaries; here the gases could nucleate to form voids. The second process could occur during periods of relatively steady operation and in fact there was some evidence that grain boundary sliding had occurred, presumably due to thermal cycling; this process could contribute to the nucleation of the voids and also to the growth of the voids into cracks.

Networks of cracks not around existing grain boundaries could have formed around previously-existing α-phase grains during earlier stages of the test. This could have been the case for specimen B-5 which cycled in and out of the β-phase many times. However the similar cracking in B-7 cannot be explained in this way as the temperature records show that there was only one occasion when β-phase operation occurred in this specimen. Thus, there may be some association of this type of cracking with previously existing β- or γ-phase grain boundaries. In this connection it is interesting to note that specimen A-6 showed a network of small voids not outlining the present grain-boundaries, and in this case there was no occasion when β-phase operation could have occurred during the test.

The gross distortion of B-3 and the lower end of B-4 was evidently due to the fact that after β- or γ- phase excursions, these specimens spent the majority of the test in the growth temperature-range. The large grains formed from the high temperature excursions could, if suitably oriented, grow out of the specimen to produce the observed effects.

4.5 General Discussion of Swelling

To enable comparison of the results obtained in this test, the swelling of the samples has been plotted against mean operating temperature in Figure 46. In this figure the volume increases of the metal (calculated from density measurements) have been normalised to a burn-up of 3000 MWd/t assuming that swelling is proportional to burn-up. The figure emphasises the markedly higher swelling obtained at the lower temperatures and the higher swelling in the specimens which had undergone β- or γ-phase operation. In the latter case some of the measured swelling could have been due to enclosed cracks and the actual swelling due to gas bubble formation may have been of the same order as in the Group I specimens. In Figure 47 the results from this test are compared with A.E.R.E. results as reported by Pugh (2). It can be seen that the Group II specimens in this test gave comparable volume increases to the Harwell specimens irradiated at lower temperatures. The Group I specimens gave volume increases comparable with the best of the A.E.R.E. results obtained on highly rated specimens (about 180 MW/t. The rating in this test was low (20 MW/t) suggesting that the high rating was not the cause of the low swelling in the A.E.R.E. specimens. The fact that the volume increases of the cracked specimens in this test lie in the central band of most of the A.E.R.E. results again demonstrates the remarkable stability of the specimens in this test.

4.6 Comparison of Behaviour of Rods and Tubes

The results of the test showed no significant overall difference between the behaviour of the rod and tube specimens; compare for instance tubes A-4 and A-6 with rods A-5 and A-7, tube A-2 with rods B-2 and B-3, and tubes B-3, B-5, B-7, and A-8 with rods B-4, B-6, and B-8. There is however some evidence that the welded ends of the hollow specimens, particularly in the Group II and Group IV specimens, were more stable than the plain ends although this could be attributed to effects due to temperature gradients. The uranium zirconium welds were very stable; only in specimen A-6 was there any cracking in the weld pool; in other cases the cracking was limited to the uranium adjacent to the weld. It is clear from Figures 40 to 45 that the weld on specimen A-6 was of a much lower quality than on all other specimens owing to a manufacturing fault. Most of the zirconium end plugs were an interference fit when assembled for welding and a "double seal" was produced during welding due to a diffusion bond forming under the main weld pool. A-6, however, was obviously not an interference fit and a poor weld was obtained.

4.7 Gas Release and Analysis

The fission gas release figures shown in Table VIII as a percentage of the total generated in each specimen, show little variation from specimen to specimen. The minimum amount was released by hollow specimen A-4 (0.14 per cent.) and the maximum by hollow specimen B-3 (1.1 per cent.).

The lowest figures recorded are about equal to the expected release of gas from the surfaces of the specimens by recoil: these were recorded for Group I specimens. Cracking in Group III and IV specimens appears to allow up to 5 times this release, most of this possibly escaping during the passage of the metal through the α/β-phase change in the early stages of the test. The low release in specimen B-4 is presumably due to the fact that only a small part of this specimen was cracked.

The full gas analysis of all inner cans which were successfully sampled is given in Table VIII. The majority of the gas in each case is helium, as expected. However, the amount of helium varies significantly from can to can. Specimens A-5 and A-7, showing 97 per cent. helium are typical expected analyses. The lowest recorded helium contents were those of cans

B-3 and B-5, (69 and 62 per cent. respectively). Both these cans, as well as others with low helium contents, showed fairly large argon, and in some cases, hydrogen contents. It is obvious that the argon came from inside the hollow rod specimens as a result of the cracking of the uranium during irradiation. The argon in these specimens was not put in intentionally; in fact, the aim during manufacture (9) had been to obtain a vacuum inside by filling with air which would have been gettered during initial heating of the test specimens. The gas analyses obtained however, show that the welding process was not successful in this aim and that large amounts of argon got into the tubes during welding. The analyses on the insides of specimens A-2 and A-4, the only two hollow specimens not to admit sodium into the bore, showed argon contents of 77 and 92 per cent. respectively. These figures must have been typical of all the hollow rod specimens. As the volume of the cavity in a hollow specimen is about ½ c.c. the pressure of gas at 0 °C appears to have been about 0.2 - 0.4 atmospheres or ½ - 1 atmosphere at operating temperature (Table VIII).

Most of the cans contained significant quantities of hydrogen. Can B-5 contained the highest amount with 23 per cent. hydrogen and 2 per cent. methane. No metallographic evidence was obtained for the presence of hydride in B-5 or any other specimen, except for that associated with cracks which is thought to have formed after irradiation during dissolution of the sodium.

The total volume of gas extracted from the inner cans is also listed in Table VIII. Generally about 0.7 to 1.0 c.c. (S.T.P.) of gas was collected from each can. As the free volume above the sodium was about 1.6 c.c. at room temperature it is apparent that the inner cans were not filled with helium at one atmosphere pressure as originally intended. It must be concluded therefore that the heat of welding expelled a significant quantity of gas. On taking the cans to operating temperature, both the sodium and the contained gas expanded and it is estimated that at 500 °C, the internal pressure was about four times the room temperature pressure. That is, the operating pressure for a can at 500 °C was in the range 2 - 3 atmospheres.

4.8 Application of Results to Fuel Element Design

Caution must be exercised in applying results obtained on small-scale highly-rated enriched test specimens to conditions existing with a power reactor fuel element. A systematic investigation of the importance of specimen size, temperature and burn-up distribution, and fuel rating has not yet been attempted, and in a test of the present type all these factors differ from those in a full-size fuel element. Nevertheless, by comparing the present results with data obtained during examination of fuel elements from the Calder and Chapelcross reactors it is possible to see how they fit into the gradually developing pattern and how they may best be used in fuel element design.

As mentioned earlier the results obtained from the Group III and Group IV specimens in this test have only limited application to fuel element performance and in the following discussion the results on specimens from Groups I and II are of principal value.

One of the most obvious and important results obtained in this test was that of peak swelling and distortion at the lower irradiation temperatures, i.e. in specimens with surface temperatures in the range 390 - 420 °C. The most highly rated Calder rods operate with a fuel surface temperature in this range and in the few which have achieved a burn-up greater than 3000 MWd/t no signs of large swelling have been found. Detailed measurements (4) on many bars show a mean volume increase of only 2.2 per cent. at 2000 MWd/t and a non-linear extrapolation of these results gives, as shown in Figure 47, a volume increase of 4.2 per cent. at 3000 MWd/t and 7.6 per cent. at 4500 MWd/t. These figures suggest that under Calder

reactor conditions swelling is less than indicated by the HIFAR Group II specimens. In part this could be due to the fact that in a Calder bar, any metal in the central region operating above 450°C should show excellent dimensional stability.

However at lower fuel temperatures the central regions may be operating within the apparently critical range and substantial distortion may occur if the fuel burn-up approaches 3000 MWd/t. In the Hunterston reactor, for example, the third element from the bottom of a flattened zone channel operates with fuel surface and centre temperatures of 339°C and 431°C respectively. This fuel element is required to achieve a mean fuel burn-up of 3310 MWd/t for a reactor average of 3000 MWd/t (i.e. for a peak burn-up of 4500 MWd/t). In view of the present results it is not inconceivable that distortion of this element may be the primary metallurgical limit to maximum channel burn-up.

Although the distortion of the Group II specimens was much more extensive than that of the Group I (or even the β-phase operation Group III specimens) it should be realised that the maximum swelling observed is still well within the civil reactor design figure of 20 per cent. even when based on the maximum changes in outer dimensions. Furthermore, the local distortion and wrinkling on the worst specimens must be fairly closely related to the grain size of the uranium rather than to specimen size and, in full-size fuel elements, this will not be scaled up proportionately and the overall volume increase will be less. Magnox cans will easily accommodate wrinkling and distortion of the magnitude observed in these specimens, even at the lowest can temperatures in a civil reactor.

The results obtained at irradiation temperatures of 460°C and above lead to considerable confidence that C.E.G.B. uranium will give an entirely acceptable performance at the higher fuel temperatures, in spite of the fact that a fuel burn-up of 4500 MWd/t is required. Recent A.E.R.E. data (S.F. Pugh, private communication) confirmed this belief by indicating only 5 - 7 per cent. volume increase after a fuel burn-up of over 5000 MWd/t at a fuel surface temperature of about 575°C. A further HIFAR metallic uranium irradiation test which was scheduled to go into the reactor in October, 1961, will check the performance of the hollow rod shape at the higher irradiation temperatures to a burn-up of 4500 MWd/t.

There have been many suggestions that certain of the more highly rated fuel elements of some of the civil reactors may suffer a brief period of β-phase operation during on-load charging owing to the can leaving the bar as a result of the differential expansion coefficients and the rapid initial rate of heating of the can. The present results indicate that the large grained structure produced by initial β-phase operation still gives an apparently acceptable performance. It is not clear however, that a badly cracked structure such as that which occurred in specimen B-5 would behave satisfactorily under power reactor conditions. End loads in the stack may cause cracked elements to deform badly and to throw high loads onto the structural components of the can. Furthermore, it is not clear what effect these cracks will have on the creep collapse of a hollow rod fuel element. Although early beta transients should be avoided if possible, it certainly cannot be stated that they should be prohibited. Beta transients occurring later in fuel element life could have different effects and the present results cannot be used to predict these. Probably later transients would give rise to considerable fission gas "sweeping up" which would cause a larger increase in overall swelling.

5. SUMMARY AND CONCLUSIONS

1. The A.A.E.C. rig using only fission heating to raise the specimen temperatures to the desired level operated satisfactorily considering the simplicity of its design. It is thought that the surface temperatures of the specimens were within 20 - 30°C of those indicated by the thermocouples during steady operation but that temperature transients giving specimen temperatures of 70 - 90°C above the indicated temperature may have occurred at reactor start-ups.

2. Both solid and hollow rod specimens irradiated in the temperature range 450 – 500 °C showed excellent stability, very low swelling (1.3 – 1.7 per cent.) and low fission gas release at burn–ups up to 0.36 per cent. of the uranium at a fuel rating of about 20 MW/t. Slow temperature drifts of up to ±20 °C and 31 shut–downs from operating temperatures to 40 °C, appear to have had little effect on the behaviour of these specimens.

3. Specimens irradiated at temperatures below 400 – 430 °C showed severe surface wrinkling and geometric distortion after burn–ups of 0.28 – 0.32 per cent. of the uranium. The maximum observed swelling (up to 8 per cent.) occurred in the specimens in this group. No explanation for this large swelling can be offered from the experimental results.

4. Due to unexplained temperature fluctuations in the early stage of the test, six of the seven specimens in stringer B and half of a specimen in stringer A underwent a period of β– phase and in some cases γ– phase operation. This resulted in a very coarse grain size which in turn resulted in gross cracking and, in specimens which subsequently operated at low temperatures, gross distortion. This cracking was generally associated with grain boundary cavities and grain boundary sliding. The results on these specimens have little direct application to reactor fuel element performance provided that early beta transients are avoided during civil reactor operation. However, it is encouraging to note that swelling in those specimens which suffered prolonged early β, or even γ– phase operation was still well within the acceptable limit.

5. No evidence was obtained from the test to indicate that hollow rod fuel elements will behave differently to solid rods. The uranium–zirconium welds showed very good stability and in certain cases actually decreased the local uranium distortion. Cracking occurred, not in the weld pool, but in the surrounding uranium rim.

6. The results obtained in this test suggest that the present power reactor design swelling allowance of 20 per cent. (i.e. 15 ± 5 per cent.) is high both for solid and hollow rod fuel elements operating in the temperature range 450 – 550 °C. However the severe wrinkling and larger volume increases which occurred in the cooler specimens suggests that the main factor limiting average fuel burn–up in a power reactor may be failure of the lower fuel elements in positions numbered two and three in the channel. The wrinkling and end dishing effects could be minimised by alloy additions and heat treatment procedures to give a truly random structure but the swelling could probably only be significantly reduced by the use of γ– phase alloys which would have an unacceptably high capture cross–section. The test has emphasised the need for more information in the apparently critical temperature range from 300 – 400 °C.

6. ACKNOWLEDGMENTS

The completion of this test in a period of little over eighteen months since its conception involved the willing cooperation of many members of the Lucas Heights staff. It is impossible to acknowledge all who have contributed to the success of the experiment but particular acknowledgment is made of the contributions of D.R. Ebeling and W.J. Turner on the engineering design of the rig; G.H. Moore, J.J. Humphreys, and D. Stevenson on the rig assembly, testing, and operation; members of the Reactor Operations Group on the rig irradiation; R.N. Whittem, M.S. Farrell, and W. Lovell on the chemical analysis and burn–up determinations; the members of the hot–cell group, particularly R. Warren and J. Mellor on the post–irradiation examination; and finally to K.F. Alder for his continual help and encouragement during the course of the test.

7. REFERENCES

1. Mercer, W.L. and Slattery, G.L. D.E.G. Memo 38(S), 1959.
2. Pugh, S.F., AERE-R 3458 1960.
3. Ratcliffe, R.J. and Hudson, B. AERE-M613, 1960.
4. Eldred, V.W. et al. NPCC/FEWP/P.648.
5. Power Reactor Technology 1, No. 2, Feb., 1958.
6. Power Reactor Technology 1, No. 1, Dec., 1957.
7. Mercer, W.L. G.E.C. Report No. 428 1961; (NPCC/FEWP/P.667).
8. Harris, D.W., D.E.G. Memo 572 (S), 1960.
9. Richards, W.G., NPCC/FEWP/P.542, 1959.
10. Turner, W.J. and Humphreys, J.J. Unpublished information, 1961.
11. McKenzie, C.D. et al. AAEC/TM64, 1960.
12. Lewis, W.B. Nucleonics, October, 1954.
13. Clough, D. (A.E.R.E.) Personal communication to W.L.Mercer.
14. Farrell, M.S. Unpublished information, 1961.
15. Whittem, R.N. Unpublished information, 1961.
16. Barwood, I.F. et al. AERE M/R 2004 1958.

TABLE I – ANALYSIS OF CASTS USED FOR MANUFACTURE OF SAMPLES

(From Reference 8)

Bar Identification	C p.p.m.	Fe p.p.m.	Al p.p.m.	O p.p.m.	H p.p.m.	N p.p.m.	Co
EML 67/1	950	$387/_{388}$	$1410/_{1357}$	190	12	10	5.00
EML 67/2	900	$396/_{375}$	1350	80	10	10	5.00
EML 67/3	950	$376/_{364}$	$1375/_{1370}$	270	13	10	–
EML 67/4	900	$377/_{359}$	$1380/_{1390}$	70	10	10	–
EML 68/1	600	$297/_{300}$	$1285/_{1255}$	60	12	5	5.06
EML 68/2	650	$303/_{295}$	$1275/_{1230}$	55	10	5	5.06
EML 68/3	625	301	$1280/_{1250}$	60	12	5	–
EML 68/4	650	$302/_{314}$	$1205/_{1275}$	75	11	5	
Accuracy of Determination	± 10%	±10%	± 5%	±20 p.p.m.	±0.1 p.p.m.	±5 p.p.m.	± 0.1

TABLE II – IN–PILE AND OUT–OF–PILE SPECIMEN POSITIONS AND NUMBERS

In–Pile Position	Type	U.K.A.E.A. No. (Ref. 8)	A.A.E.C. No.	Corresponding Out–of–pile Specimen	
				U.K.A.E.A. No. (Ref. 8)	A.A.E.C. No.
A–2	Tube	EML/68/1/1	86	EML/68/1/2	93
B–2	Rod	EML/67/1/2	72	EML/67/1/4	79
A–3	Rod	EML/67/1/5	73	EML/67/2/1	80
B–3	Tube	EML/68/1/3	87	EML/68/1/4	94
A–4	Tube	EML/68/2/1	88	EML/68/2/3	95
B–4	Rod	EML/67/2/3	74	EML/67/2/4	81
A–5	Rod	EML/67/2/5	75	EML/67/3/1	82
B–5	Tube	EML/68/2/4	89	EML/68/3/1	96
A–6	Tube	EML/68/3/2	90	EML/68/3/3	97
B–6	Rod	EML/67/3/2	76	EML/67/4/3	85
A–7	Rod	EML/67/3/5	77	EML/67/3/6	84
B–7	Tube	EML/68/3/5	91	EML/68/3/4	98
A–8	Tube	EML/68/4/3	92	EML/68/4/4	99
B–8	Rod	EML/67/4/1	78	EML/67/3/3	83

TABLE III – SUMMARY OF INDICATED TEMPERATURES DURING OPERATION

Specimen No.	Thermocouple Position	Desired Temperature	Peak Indicated Thermocouple Temperature During Period of Fluctuating Temperatures	Period of Steady Operation			Remarks
				Range for 95% of Period	Estimated Mean	Peak Temperature	
A–2 tube	Upper Lower	410	400 400	370–420 360–380	400 370	430 400	Temperatures very steady throughout.
B–2 rod	Upper Lower	410	410 415	330–390 340–390	350 370	390 400	,, ,, ,, ,,
A–3 rod	Upper Lower	440	440 425	380–440 370–420	410 395	450 435	,, ,, ,, ,,
B–3 tube	Upper Lower	440	775 715	380–550 400–440	430 410	550 440	Probable γ–phase operation.
A–4 tube	Upper Lower	470	435 435	420–450 400–430	435 420	460 450	Very steady operation.
B–4 rod	Upper Lower	470	756 728	360–430 400–550	395 460	450 555	Definite β–phase operation probably gamma.
A–5 rod	Upper Lower	500	450 470	420–450 450–480	435 465	460 500	Fairly steady operation.
B–5 tube	Upper Lower	500	685 625	430–550 410–520	510 460	555 540	Cycled into beta many times at early stage and continued cycling at lower temperatures for most of test.
A–6 tube	Upper Lower	530	525 455	390–420 420–450	400 440	420 460	Steady operation. Some initial fluctuations recorded on upper thermocouple.
B–6 rod	Upper Lower	530	770 745	460–540 490–540	495 505	560 555	Possible γ–phase operation. Cycled from beta to alpha five times at shut–downs in first 13 days.
A–7 rod	Upper Lower	560	510 495	490–520 470–490	505 480	530 500	Very steady operation.
B–7 tube	Upper Lower	560	485 580	460–490 450–510	475 480	500 520	Wide discrepancies between upper and lower thermocouples during early stages of test. Metallographic work showed β–phase operation.
A–8 tube	Upper Lower	590	580 545	540–580 510–530	560 520	600 535	Steady operation, metallographic examination showed β–phase operation of upper part of specimen.
B–8 rod	Upper Lower	590	500 670	490–520 440–530	490 470	520 540	Brief β–phase operation. Wide discrepancies between upper and lower thermocouples during early stages of test.

TABLE IV – BURN-UP OF SPECIMENS EXPRESSED AS PERCENTAGE OF TOTAL URANIUM WHICH HAS FISSIONED

Specimen	Method 1*	Method 2	Method 3	Method 4
A–2	0.31	0.27	0.29	
B–2	0.31	0.28	0.30	
A–3	0.33	0.31	0.33	
B–3	0.33	0.31	0.33	
A–4	0.36	0.35	0.37	
B–4	0.36	0.33	0.35	
A–5	0.37	0.33	0.35	
B–5	0.37	0.33	0.35	
A–6	0.36	0.34	0.36	0.37
B–6	0.36	0.35	0.37	0.36
A–7	0.35	0.32	0.34	
B–7	0.35	0.33	0.35	
A–8	0.32	–	–	
B–8	0.32	0.31	0.33	
Estimated Error	±0.04	±0.04	±0.04	±0.015

* See text for explanation of methods used, (Section 3.1).

TABLE V – SUMMARY OF RESULTS OF MACRO EXAMINATION

Group No.	Specimen No.	Cracking	Wrinkling	End Effects	Weld Cracking	Bore	Figure No.	Remarks
I	A–4 tube	None	Slight	None	None	Unaffected (no sodium)	12	
	A–5 rod	None	Trace	None	–	–	11	
	A–6 tube	Fine at lower end	Trace	None	Slight circum–ferential	Sodium present	10	
	A–7 rod	None	None	None	–	–	9	
II	B–2 rod	None	Severe	Dishing at both ends	–	–	15	Side bulging associated with dished ends.
	A–2 tube	None	Severe	Dishing at lower end	Slight circum–ferential in uranium near weld	Wrinkled (no sodium)	13	"
	A–3 rod	None	Severe	Dishing at both ends	–	–	14	"
III	A–8 tube	Moderate	None	None		Sodium present	16	
	B–8 rod	A few wide cracks	Trace	None	–	–	17	
	B–7 tube	Extensive	None	None		Sodium present	18	
	B–6 rod	Extensive	None	None	–	–	19	
	B–5 tube	Extensive	None	None		Sodium present	20	
IV	B–3 tube	Extensive particularly at lower end	Gross distortion at lower end	None		Sodium present	21	Partial collapse of wall occurred on one side.
	B–4 rod	Extensive at lower end only	Slight at upper end. Gross distortion at lower end	None		–	22	

increasing

TABLE VI – DIMENSIONS AND DIMENSIONAL CHANGES

Group Number	Specimen Number	Dimensions Before Irradiation (Inches)			Dimensions After Irradiation (Inches)					Dimensional Changes in Percent			
		Outside Diameter	Height	Inside Diameter of Tubes	Outside Diameter		Height		Inside Diameter of Tubes (approx.)	Mean Outside Diameter %	Mean Height %	Inside Diameter %	Overall Volume of Specimens %
					Range	Mean	Range	Mean					
I	A7 rod	0.2527	0.7871	–	0.2537 – 0.2544	0.254	0.7889 – 0.7892	0.789	–	0.6	0.2	–	1.4
	A6 tube	0.3943	0.789	0.235	0.3968 – 0.3983	0.398	0.7939 – 0.7941	0.794	0.238	0.8	0.6	1.3	2.2
	A5 rod	0.2534	0.7868	–	0.2551 – 0.2563	0.256	0.790 – 0.792	0.792	–	0.9	0.6	–	2.4
	A4 tube	0.3940	0.788	0.235	0.3981 – 0.4025	0.400	–	0.800	0.232–0.234	1.4	1.6	(0.5 to 1.3)	4.5
II	A3 rod	0.2531	0.7884	–	0.257 – 0.263	0.259	0.792 – 0.805	0.797	–	2.4	1.1	–	6.0
	A2 tube	0.3940	0.787	0.234	0.413 – 0.423	0.417	0.825 – 0.828	0.826	0.236	5.8	5.0	0.9	(17)
	B2 rod	0.2533	0.7880	–	0.267 – 0.274	0.271	0.775 – 0.801	0.787	–	7.0	–0.1	–	(14)
III	A8 tube	0.3938	0.784	0.233	0.4010–0.4029	0.402	0.7977–0.7979	0.798	0.238	2.1	1.8	2.1	6.1
	B8 rod	0.2504	0.7875	–	0.253 – 0.254	0.2535	0.798 – 0.799	0.798	–	1.2	1.4	–	3.8
	B7 tube	0.3941	0.790	0.235	0.4035 – 0.406	0.4045	0.807 – 0.808	0.8075	–	2.6	2.2	–	7.6
	B6 rod	0.2525	0.7879	–	0.256 – 0.259	0.257	0.803 – 0.807	0.804	–	1.9	2.0	–	5.9
	B5 tube	0.3945	0.7875	0.235	0.403 – 0.407	0.406	–	0.808	0.238	2.8	2.6	1.3	8.4
IV	B4 rod	0.2525	0.7849	–	0.258 – 0.260	0.259	–	–	–	2.5	–	–	–
	B3 tube	0.3941	0.786	0.235	0.383 – 0.406	0.399	0.814 – 0.816	0.815	–	1.2	3.7	–	6.2

NOTES: (i) The overall volume increase of specimens was calculated from the mean outer dimensions.

(ii) The extent of dishing in tube A2 was 0.016 inch; in rod B2, 0.021 inch and 0.011 inch; and in rod A3, 0.007 inch 0.002 inch.

TABLE VII – DENSITIES, DENSITY CHANGES, AND SWELLING OF SPECIMENS

Group No.	Specimen No.	Density Before Irradiation		Density After Irradiation		% Change in Density		% Change in Volume of Metal
		Specimen	Metal	Specimen	Metal	Specimen	Metal	
I	A7 rod	–	18.62	–	18.32	–	1.6	1.6
	A6 tube	–	18.57	–	18.25	–	1.7	1.7
	A5 rod	–	18.54	–	18.30	–	1.3	1.3
	A4 tube	12.67	18.51	12.32	18.27	2.7	1.3	1.3
II	A3 rod	–	18.63	–	18.23	–	2.2	2.3
	A2 tube	12.62	18.74	11.64	17.35	7.9	7.4	8.0
	B2 rod	–	18.66	–	17.71	–	5.1	5.4
III	A8 tube	–	18.58	–	18.11	–	2.5	2.6
	B8 rod	–	18.63	–	18.38	–	1.3	1.3
	B7 tube	–	18.6 ±0.1	–	18.17	–	2.5	2.6
	B6 rod	–	18.62	–	18.00	–	3.3	3.4
	B5 tube	–	18.6 ±0.1	–	18.03	–	3.3	3.4
IV	B4 rod	–	18.61	–	17.77	–	4.5	4.7
	B3 tube	–	18.81	–	17.96	–	4.5	4.7

NOTE: For tubes, the columns headed specimen density give the apparent density of the whole specimen and the columns headed metal density give the density of the uranium determined after sectioning off the welded end of the tube. The pre-irradiation metal densities for B5 and B7 are estimates as these were not measured.

TABLE VIII – RESULTS OF GAS ANALYSIS

Group No.	Specimen No.	Composition of Gas (Percent by Volume)								Total Content of gas c.c. at S.T.P.	Amounts of Xe and Kr (c.c. at S.T.P.x 10^4)											
		He	H_2	$CO+N_2$	O_2	A	CO_2	CH_4	Xe+Kr		Kr83	Kr84	Kr85	Kr86	Total Kr	Xe131	Xe132	Xe133	Xe134	Xe136	Total Xe	Total Xe+Kr
I	A7 rod	97.2	0.7	0.8	0.3	0.3	0.3	0.2	0.17	0.88	0.3	0.6	0.5	2.3	3.7	1.1	2.1	0.8	3.3	4.4	11.7	15.4
	A6 tube	86.0	0.9	4.7	1.4	3.6	0.04	0.05	0.31	1.07	0.6	1.1	0.3	2.1	4.1	3.1	6.4	1.8	7.2	10.0	28.5	32.6
	A5 rod	97.7	0.9	0.4	0.1	0.6	0.04	0.02	0.23	1.07	0.4	1.0	1.9	1.7	5.0	2.1	3.1	–	6.1	8.3	19.6	24.6
	A4 tube	95.0	1.9	0.5	0.1	2.1	0.05	0.1	0.28	0.84	0.4	0.8	0.2	1.7	3.1	1.8	3.4	–	6.1	8.0	19.3	22.4
II	A4 (inside tube)	n.d.	4.5	2.1	0.5	91.6	0.2	0.9	0.08	0.076	0.04	0.04	0.04	0.04	0.16	0.05	0.08	–	0.11	0.17	0.41	0.57
	A2 (inside tube)	n.d.	15.1	2.8	0.6	76.9	0.9	3.5	0.05	~0.2	0.02	0.02	0.06	0.06	0.16	0.10	0.12	–	0.26	0.30	0.78	0.94
III	A8 tube	77.1	2.9	0.5	0.2	17.8	0.1	0.1	1.05	0.84	1.7	3.4	1.0	6.2	12.3	6.6	9.6	–	26	34	76.2	88.5
	B8 rod	88.8	2.4	2.7	1.4	4.1	0.1	0.1	0.39	0.61	0.5	0.9	0.3	1.6	3.3	2.1	3.7	0.9	5.6	8.2	20.5	23.8
	B5 tube	62.3	22.8	2.3	0.4	9.0	0.4	2.2	0.64	0.72	0.9	1.6	0.3	3.9	6.7	4.1	6.5	0.9	12.0	16.0	39.5	46.2
IV	B4 rod	96.6	1.8	0.6	0.2	0.5	0.04	0.07	0.21	1.07	0.3	0.6	0.1	1.6	2.6	2.1	3.4	–	6.0	8.3	19.8	22.4
	B3 tube	69.2	2.2	0.6	0.1	26.3	0.1	0.1	1.6	0.99	3.2	5.6	1.7	20.0	30.5	15	20	–	40	53	128	158.5

TABLE IX – FISSION GAS RELEASE

Group No.	Specimen No.	Weight Uranium (g)	Percent U235 (g)	Weight U235 (g)	Fraction of Atoms Fissioned (p)	Measured Gas Release (V) c.c. (S.T.P.)	$\frac{A}{2.24y}$ (Reference 16)	Percent Gas Released $\frac{VfA}{2.24py}$	Comments
I	A7 rod	11.90	3.60	0.428	0.00342	0.0015	$\frac{1}{0.2277}$	0.16	
	A6 tube	19.40	3.64	0.706	0.00357	0.0032	"	0.20	
	A5 rod	11.94	3.60	0.430	0.00357	0.0025	"	0.25	
	A4 tube	19.62	3.64	0.714	0.00355	0.0022	"	0.14	
II	A3 rod	12.02	3.60	0.433	0.00329	–	"	–	No pressure rise recorded.
	A2 tube	19.54	3.64	0.711	0.00311	–	"	–	Equipment fault.
	B2 rod	12.02	3.60	0.433	0.00308	–	"	–	" "
III	A8 tube	19.07	3.64	0.694	0.00323	0.0088	"	0.63	
	B8 rod	11.70	3.60	0.422	0.00320	0.0024	"	0.28	
	B7 tube	19.45	3.64	0.708	0.00345	–	"	–	
	B6 rod	11.96	3.60	0.431	0.00353	–	"	–	No analysis attempted, air leak in rig gave unreliable results.
	B5 tube	19.59	3.64	0.713	0.00361	0.0046	"	0.29	
IV	B4 rod	11.83	3.60	0.426	0.00351	0.0022	"	0.23	
	B3 tube	19.49	3.64	0.708	0.00333	0.016	"	1.1	

TABLE X – SUMMARY OF RESULTS OF METALLOGRAPHIC EXAMINATION

Group No.	Specimen No.	Grain Structure	Cracking and Porosity	Weld	General Remarks	Refer to Figure No.
I	A7 rod	Unchanged. Fine irregular grains – no twinning.	None	–	No optically observable effects due to irradiation	26
	A6 tube	Unchanged in walls. Grain shape more regular on lower end although still fine – no twinning.	None in walls. Fine inter-granular cracking at lower end, together with a network of pores not associated with grain boundaries.	Sound on one side. Weld metal cracked on other side.	Walls of tube similar to A7. Bottom end shows slight crack-ing and porosity.	27 & 40
	A5 rod	NOT EXAMINED				
	A4 tube	Fine irregular grains. Unchanged except for some twinning towards outer surface.	None	Sound	Similar to A7 except for twinning towards the outer surface.	28 & 41
II	A3 rod	NOT EXAMINED				
	B2 rod	Grain size unchanged. Extensive complex twinning, greater on out-side, so grains became almost indistinguishable.	None	–	No optical evidence of porosity. Specimen difficult to prepare, prone to pitting, and difficult to reveal grain structure in polar-ised light. Wrinkling is on larger scale than grain size and difficult to associate protuber-ances with single grains or even groups of grains.	30
	A2 tube	As for B2	None	–	As for B2	29
III	A8 tube	Unchanged on bottom. Changed on walls to coarse columnar structure. Fig. 31(c) and then to coarse equi-axed structure Fig. 32(a)	None on bottom. Extensive intergranular cavities in coarse grained regions de-veloping into intergranular cracks.	Sound	The transition in structure along the wall shows that the upper part of the specimen was heated into the β-phase. Note the grain boundary sliding in Fig.32 (d).	31, 32, & 42
	B7 tube	Variable. Mainly coarse grained at bottom (single grains across section) with fine grains at inner surface. Mixed grain-size on walls but coarser than original.	Network of coarse cracks not associated with grain bound-aries except at bottom. Net-work of cavities on walls again seldom associated with grain boundaries.	Extensive crack across weld metal on one side.	Very complex. Clearly shows evidence of one and perhaps two excursions into the β-phase.	33, 34, & 43

Table X Continued

TABLE X – SUMMARY OF RESULTS OF METALLOGRAPHIC EXAMINATION (continued)

Group No.	Specimen No.	Grain Structure	Cracking and Porosity	Weld	General Remarks	Refer to Figure No.
III	B6 rod	Medium to coarse–grained–columnar at outside surface, equi–axed in centre.	Intergranular cavities develop–ing into cracks mainly assoc–iated with present grain–boundaries.	–	Evidence of high–temperature operation followed by slow–cooling.	35
	B5 tube	Coarse grained with few sub–boundaries.	Coarse net–work of cavities and cracks seldom associated with present grain boundaries, yielding massive displacements at surface.	Sound	Evidence for two excursions into the β–phase, one early and one late in the operating period.	36, 44
	B8 rod	Coarse grained with well defined sub–grain and very irregular grain boundaries.	Some cavities mainly around obvious grain boundaries. Some tears across grains.	–	No explanation why this specimen should have different structure from B5, B6, and B7.	37
IV	B3 tube	Very coarse grain size with fine precipitate preferentially orientated within grains.	Coarse cracks and network of cavities. Displacements at surface associated with cracks.	Extensive crack in uranium and marked inter–diffusion.		38, 45
	B4 rod	Medium to coarse grain size with fine precipitate prefer–entially orientated in grains.	None	–	The sections examined were taken from the sound end of this specimen. Presumably the other end would show effects similar to B3.	39

TABLE XI – SUMMARY OF RESULTS

Group No.	Specimen No.	Highest Recorded Temperature	Mean Thermocouple Temperature During Steady Operation	Burn–up	Macro Appearance	Microstructure	Volume Change of Metal Calculated from Densities (%)	Overall Volume Change of Specimen Calculated from outer Dimensions (%)	Fission Gas Release (%)
I	A–7 rod	Upper 530	505	0.32 – 0.35	Unaltered.	Unchanged.	1.6	1.4	0.16
		Lower 500	480						
	A–6 tube	525	400	0.36 – 0.38	Very fine cracking otherwise unaltered.	Fine grain, fine intergranular cracking at lower end.	1.7	2.2	0.2
	A–5 rod	460 497	435 465	0.35 – 0.37	Virtually unaltered.	Not examined.	1.3	2.4	0.25
	A–4 tube	460 450	435 420	0.35 – 0.37	Slight wrinkling.	Grain–size fine and unchanged, some twinning	1.3	4.5	0.14
II	A–3 rod	450 435	410 395	0.31 – 0.33	Severe wrinkling.	Not examined.	2.3	6.0	–
	A–2 tube	430 405	400 370	0.27 – 0.31	Severe wrinkling.	Fine grain. Heavily twinned.	8.0	(17)	–
	B–2 rod	410 415	350 370	0.28 – 0.31	Severe wrinkling.	Fine grain. Heavily twinned.	5.4	(14)	–
III	A–8 tube	605 545	560 520	0.32	Cracking on walls.	Coarse grained on walls, fine grained at bottom.	2.6	6.1	0.63
	B–8 rod	520 672	490 470	0.31 – 0.33	A few wide cracks.	Coarse grain.	1.3	3.8	0.28
	B–7 tube	485 580	475 480	0.33 – 0.35	Some cracking.	Coarse grain in some areas.	2.6	7.6	–
	B–6 rod	770 745	560 555	0.36 – 0.37	Severe cracking.	Coarse grain.	3.4	5.9	–
	B–5 tube	685 625	510 460	0.33 – 0.37	Severe cracking.	Coarse grain.	3.4	8.4	0.29
IV	B–4 rod	756 730	395 460	0.33 – 0.36	Severe cracking and distortion at lower end.	Coarse grain.	4.7	–	0.23
	B–3 tube	775 715	430 410	0.31 – 0.33	Severe cracking and distortion at lower end.	Coarse grain.	4.7	6.2	1.1

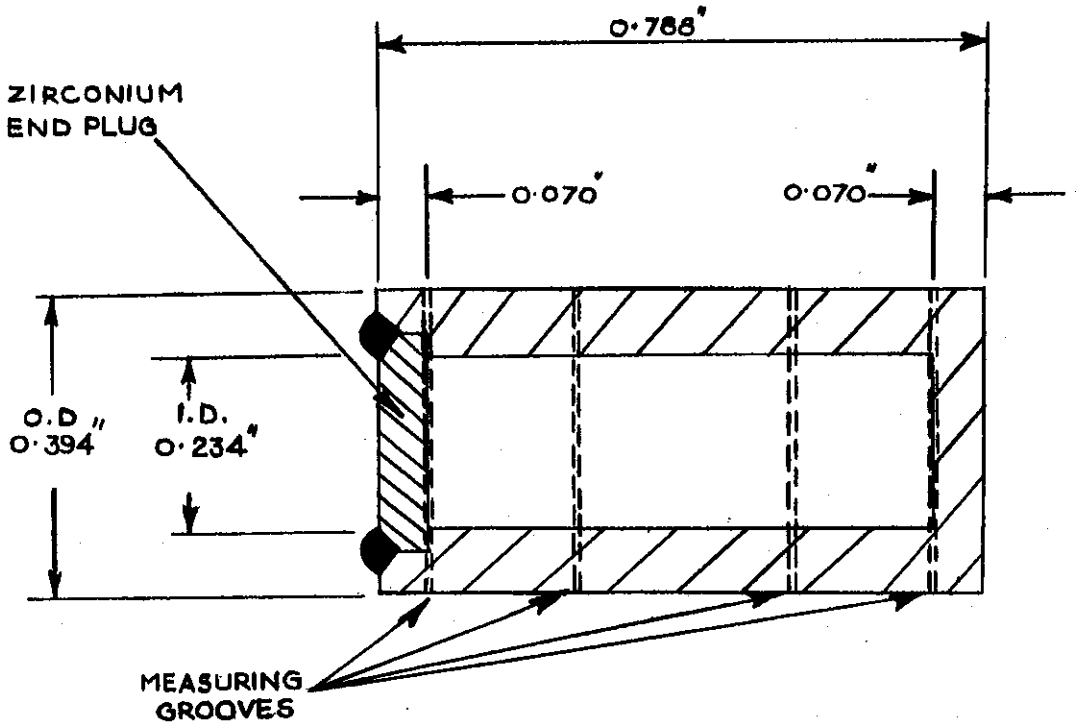

HOLLOW ROD

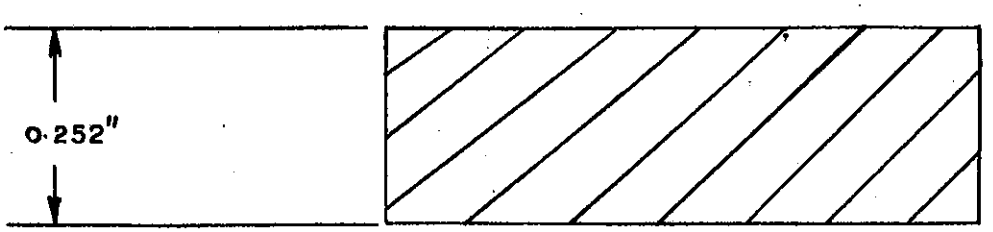

SOLID ROD

FIGURE 1 FINAL NOMINAL DIMENSIONS OF TEST SPECIMENS

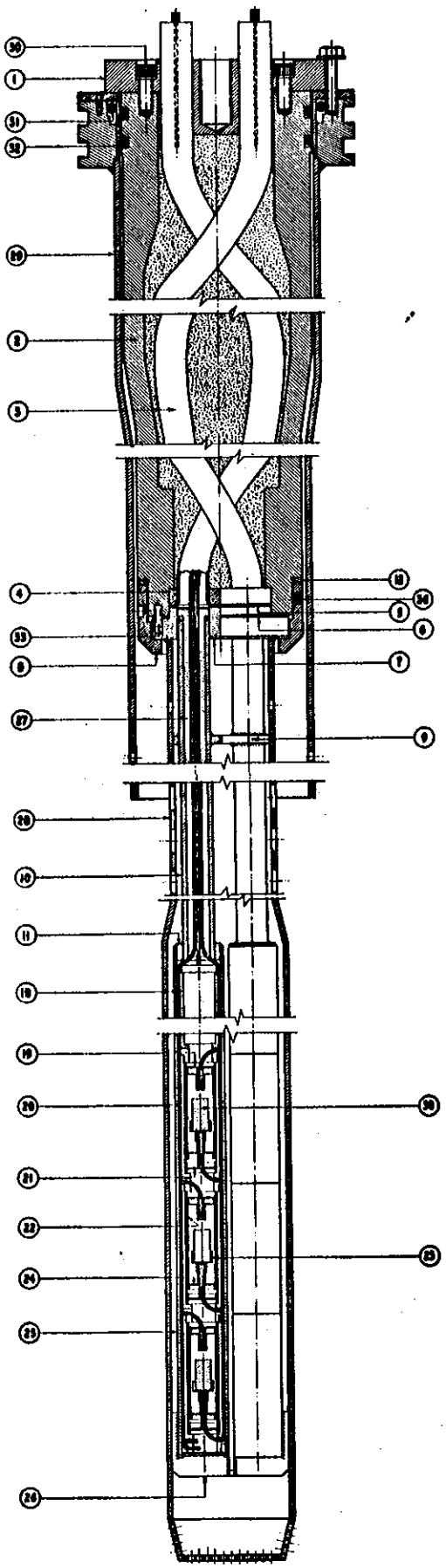

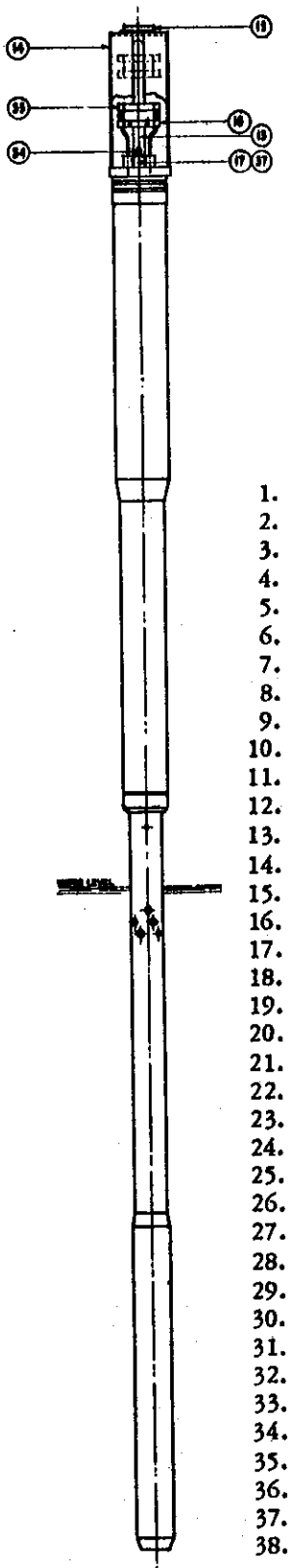

1. Top Plate
2. Plug
3. Through Plug Tubes
4. Tube Locating Plate
5. Washer
6. Washer
7. Locating Plate
8. Clamping Ring
9. Tube Guide
10. Spacer Tube
11. Tube Reducer
12. Sealing Washer
13. Lifting Bolt and Terminal Block Holder
14. Cover
15. Clamping Nut
16. Thermocouple Clamping Plate
17. Purging Tube Adaptor
18. Aluminium Former
19. Stainless Steel Can End
20. Stainless Steel Can Outer Casing
21. Stainless Steel Can End
22. Sodium Capsule Outer Casing
23. Zirconium Cup
24. Sodium Capsule End
25. Experimental Former
26. Spacing Fins
27. Thermocouple Former
28. Outer Casing
29. 4V Thimble
30. 'Unbrako' Capscrews
31. 'O' Ring
32. 'O' Ring
33. Dowel
34. Lockheed Coupling
35. Terminal Blocks
36. Grubscrew
37. 'Unbrako' Screws
38. Specimen

FIGURE 2 GENERAL ARRANGEMENT OF IRRADIATION RIG

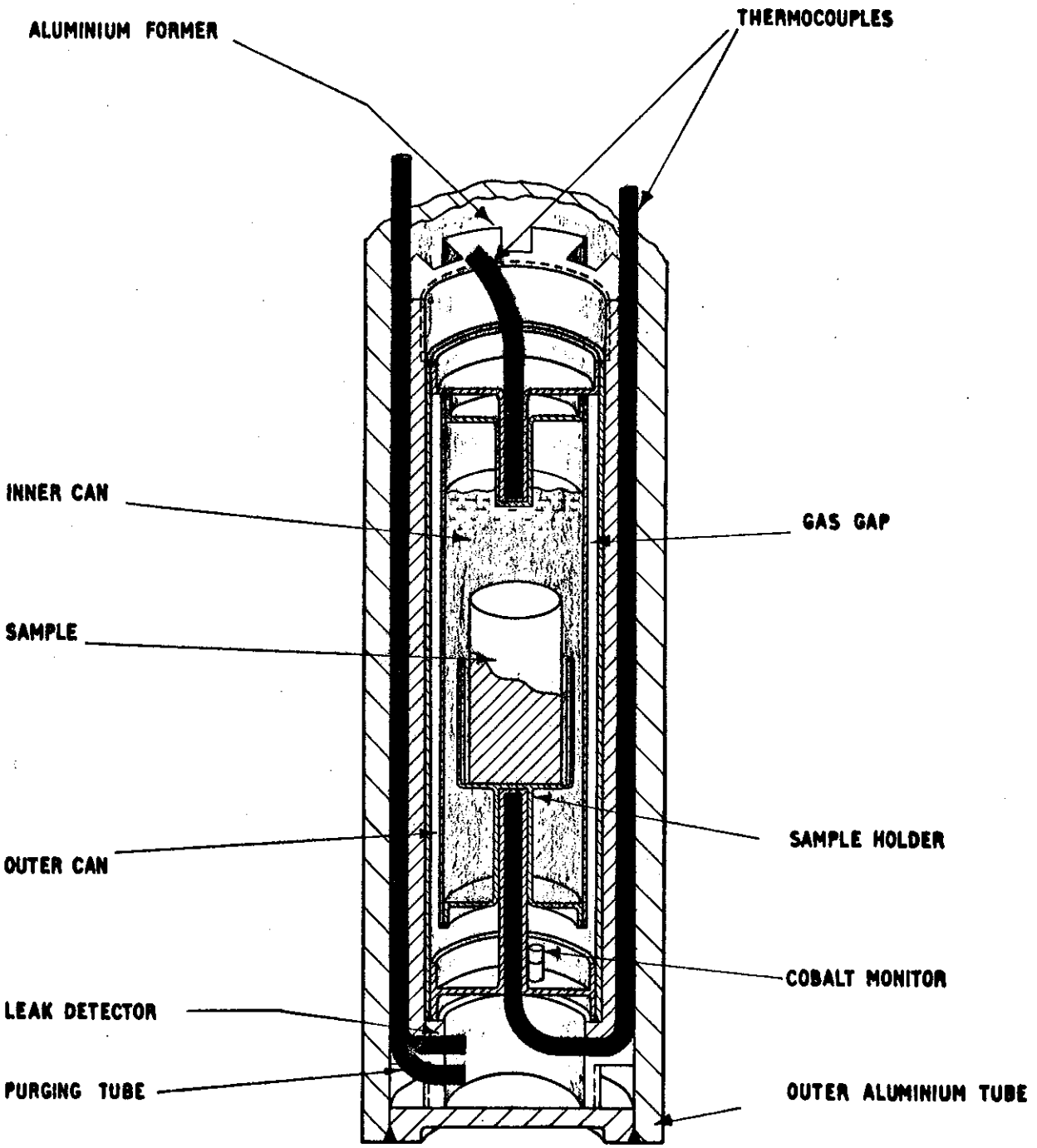

FIGURE 3 SCHEMATIC CROSS-SECTION OF IRRADIATION CAN

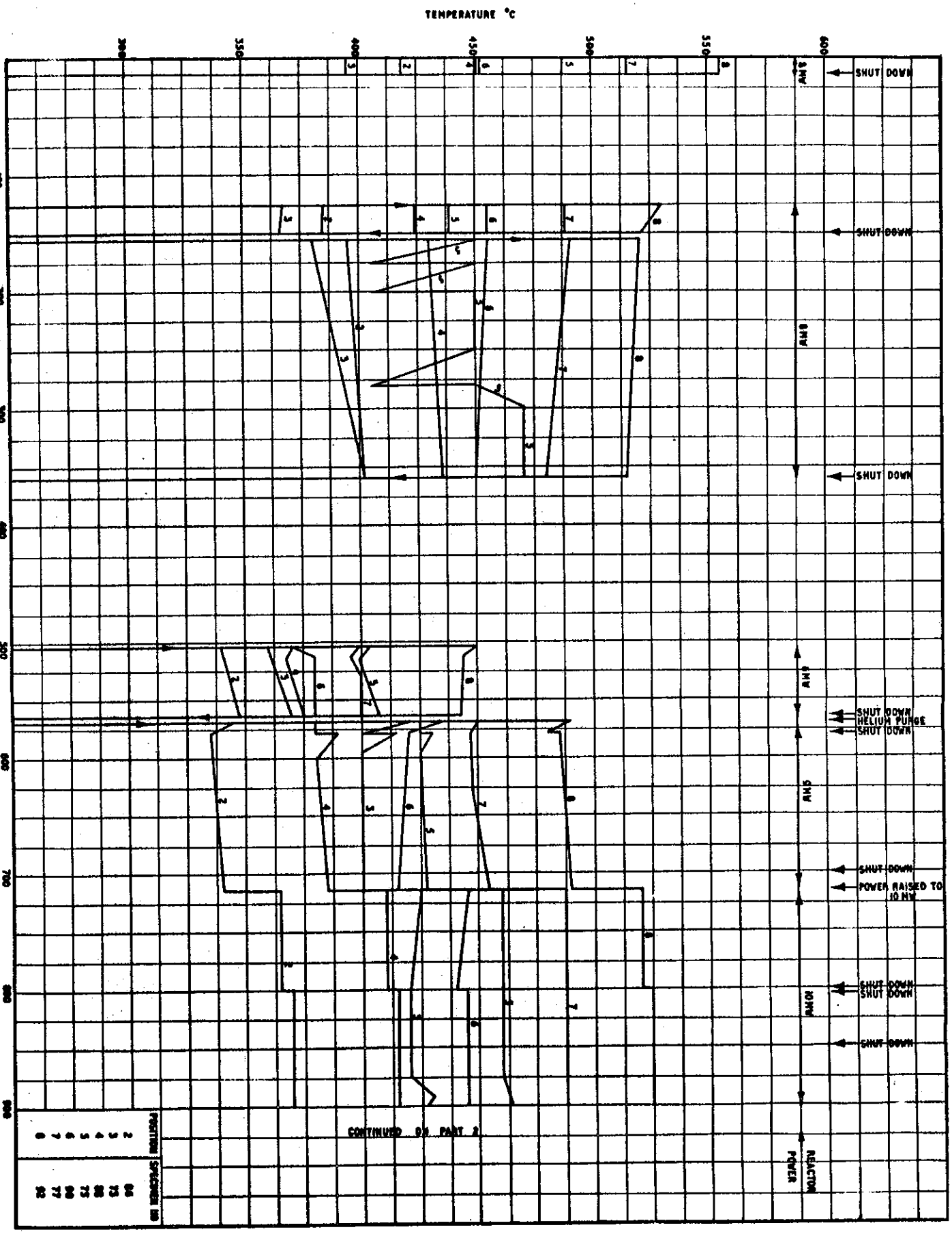

FIGURE 4 TEMPERATURE CHART STRINGER A — PART 1

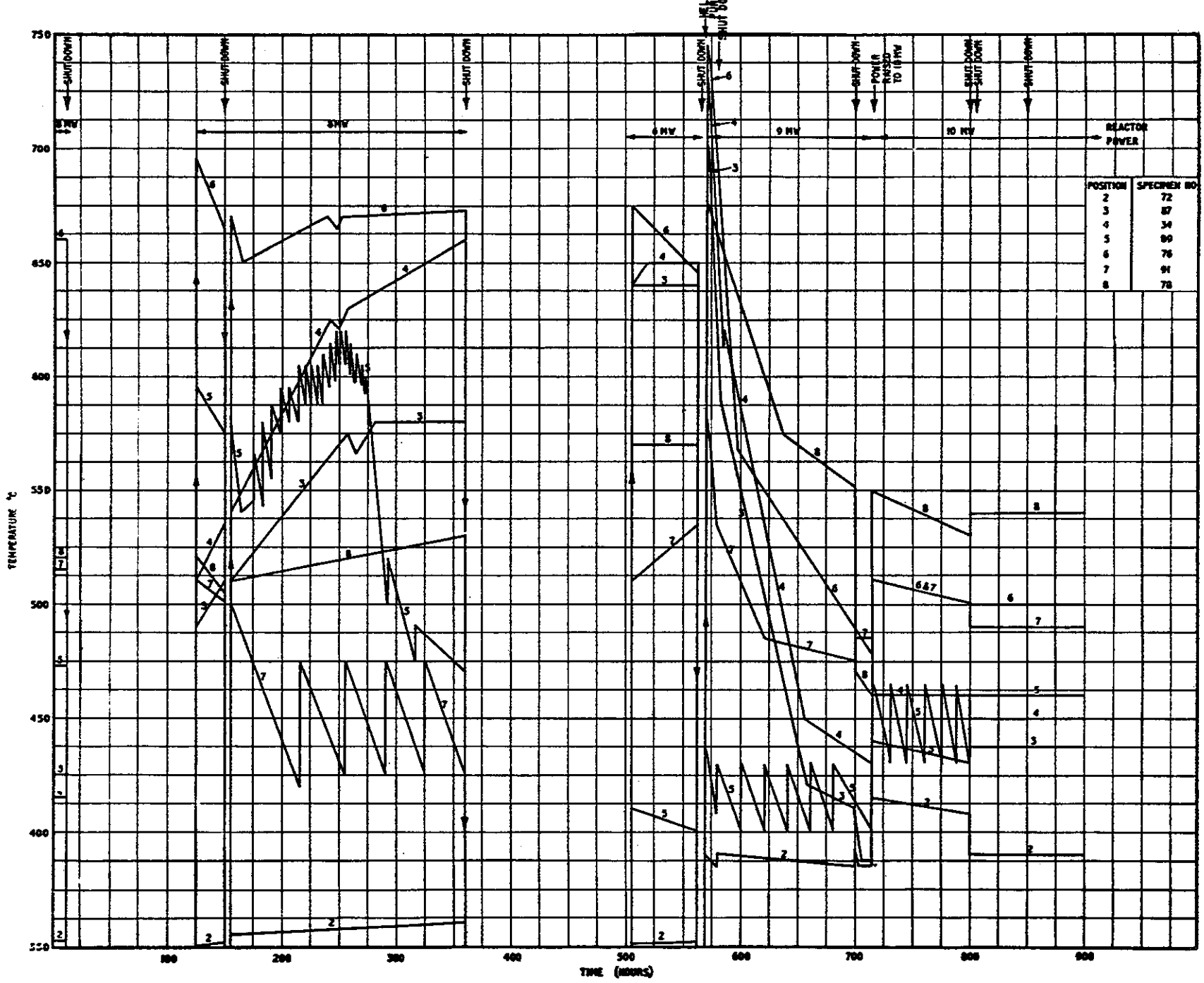

FIGURE 5 TEMPERATURE CHART
STRINGER B — PART 1

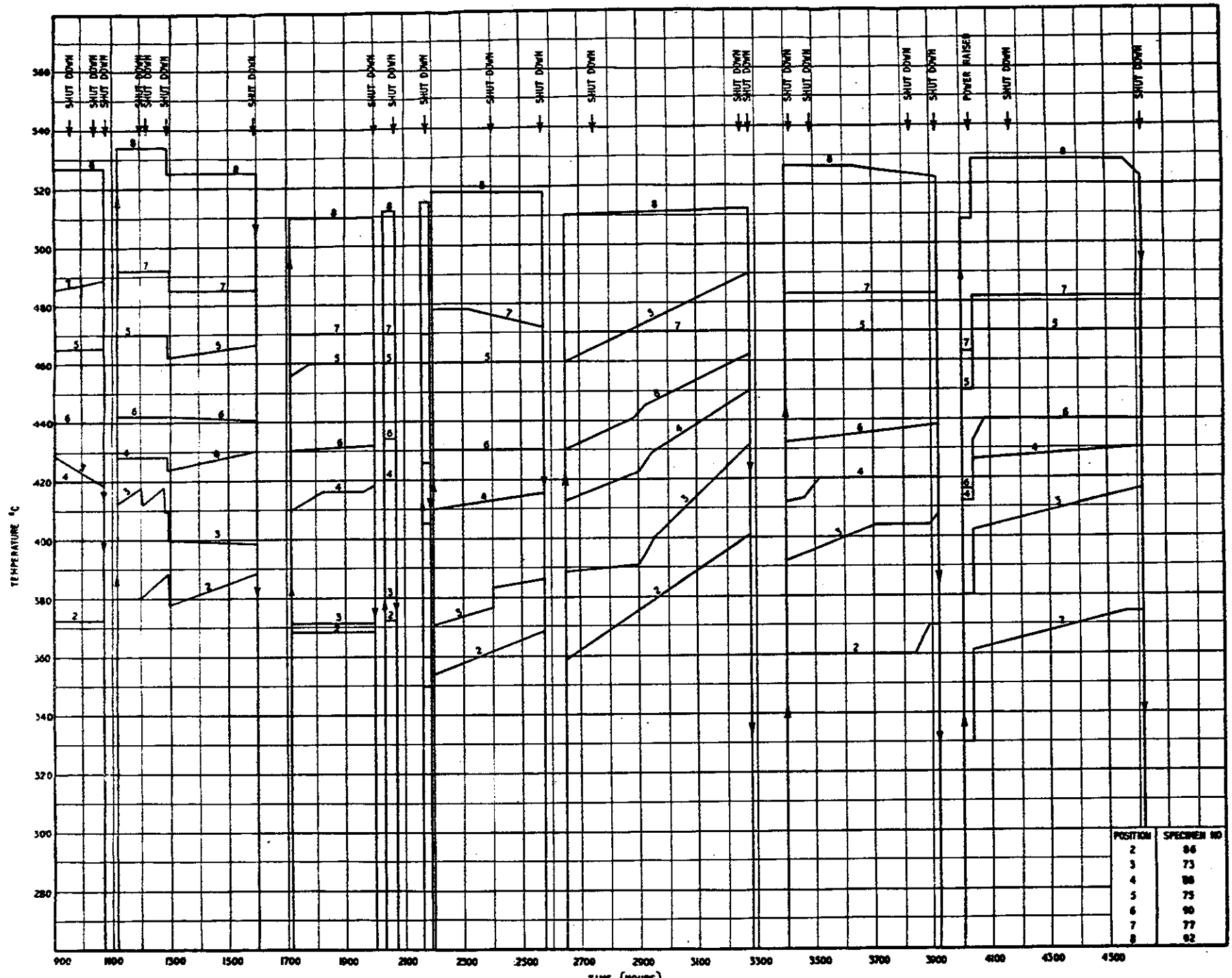

FIGURE 6 TEMPERATURE CHART – STRINGER A PART II

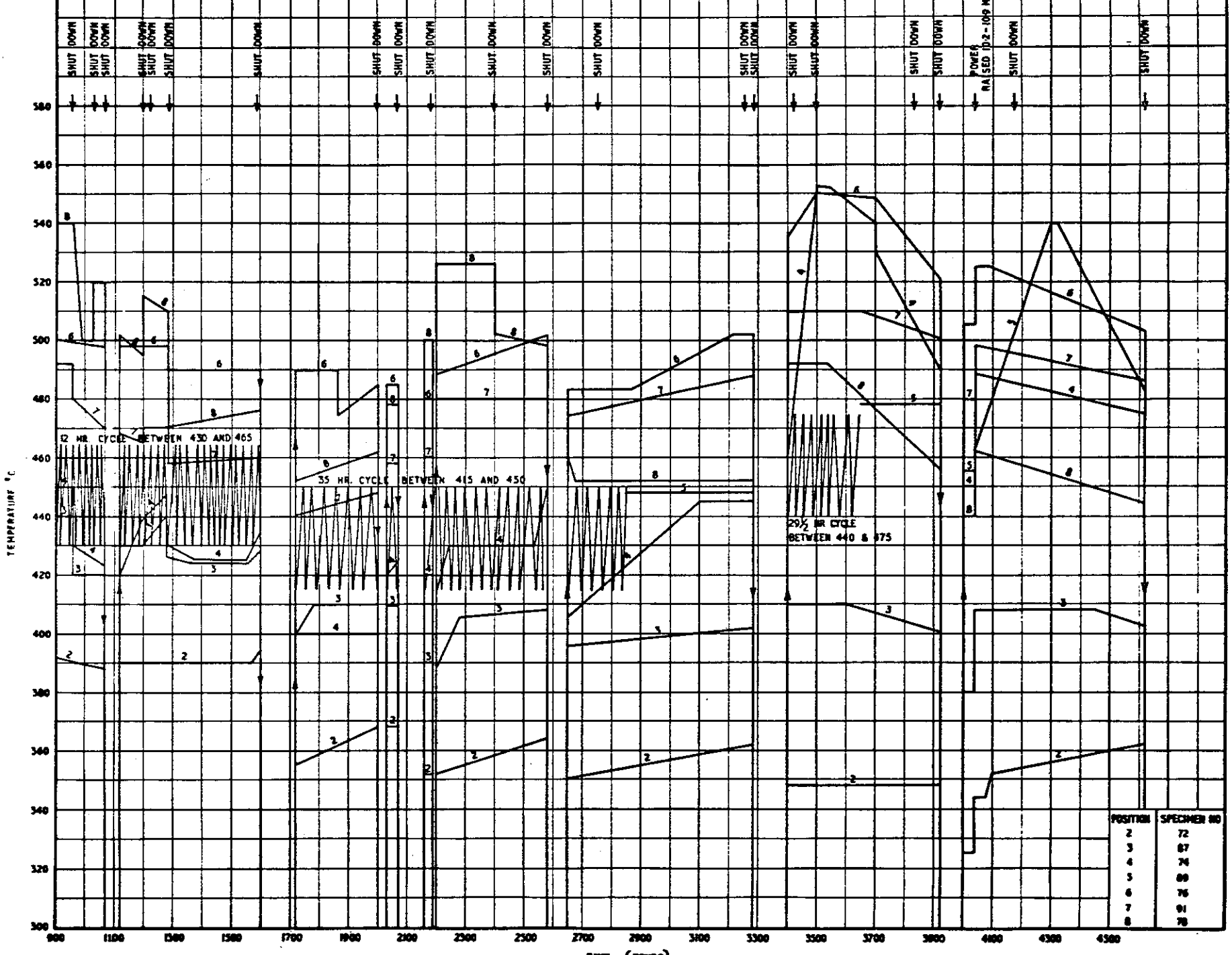

FIGURE 7

TEMPERATURE CHART — STRINGER B
PART II

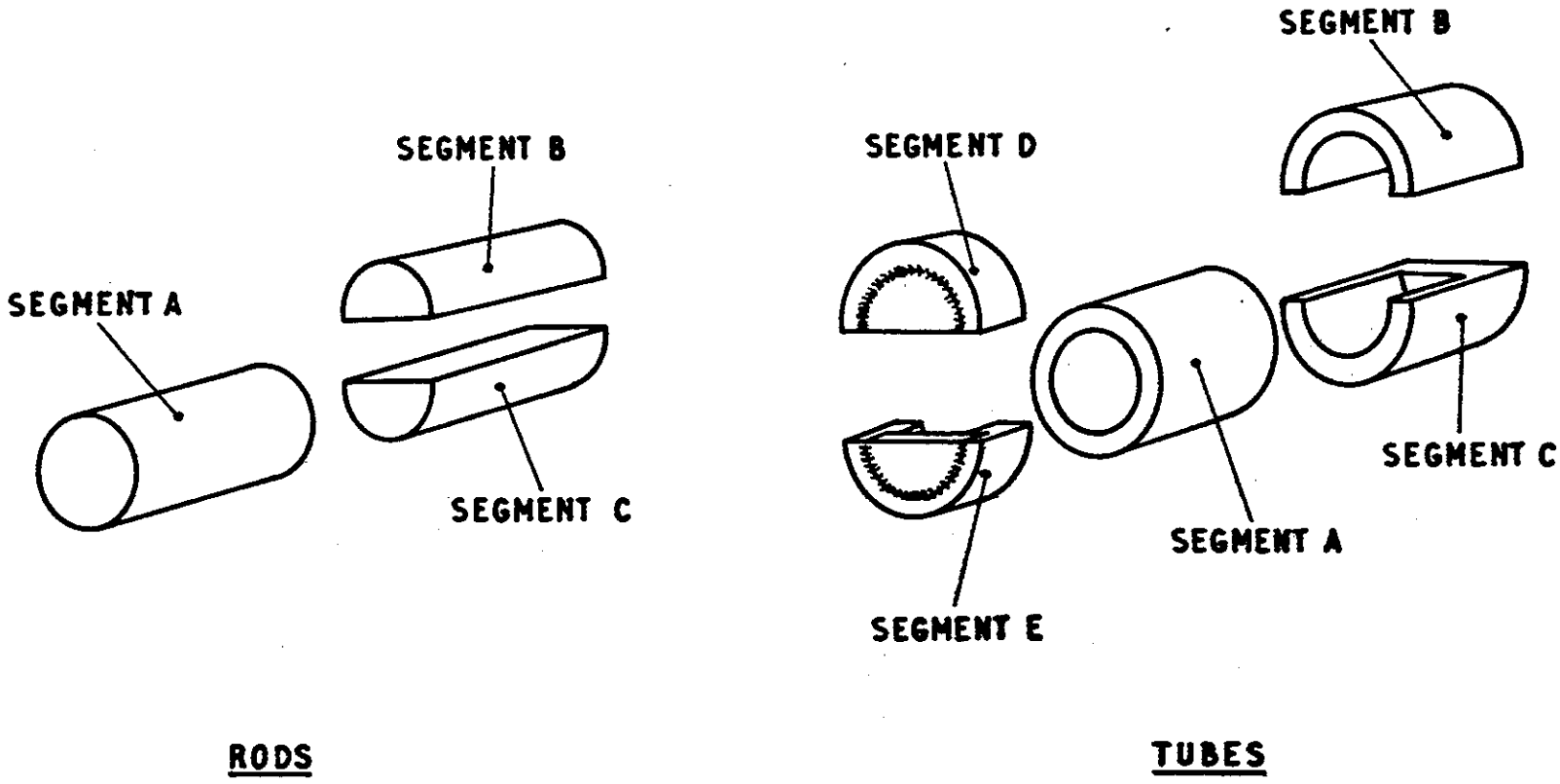

FIGURE 8 SKETCH SHOWING SECTIONING OF SPECIMENS

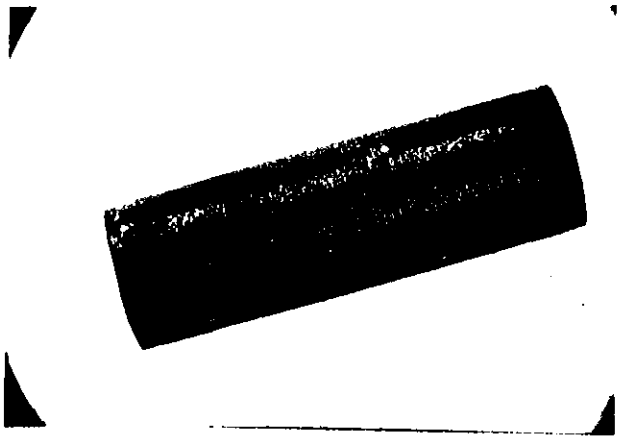

(A) X 2

(A) X 2

(B) X 6

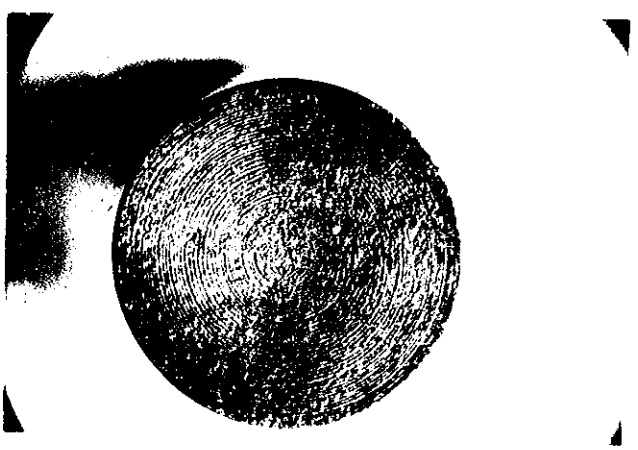

(B) X 3

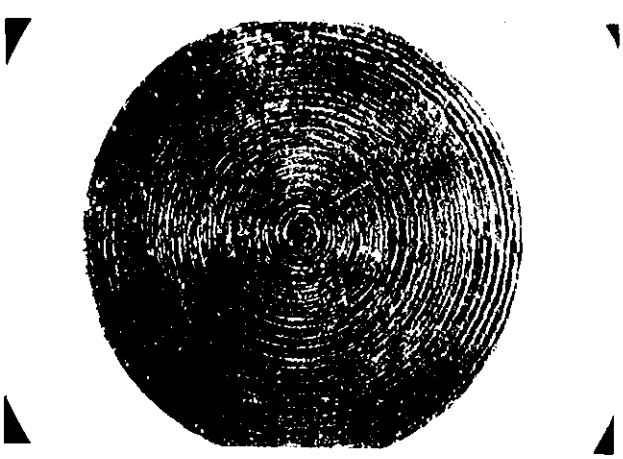

(C) X 6
SOLID ROD
A7

FIG.9

(C) X 6
HOLLOW ROD
A6

FIG.10

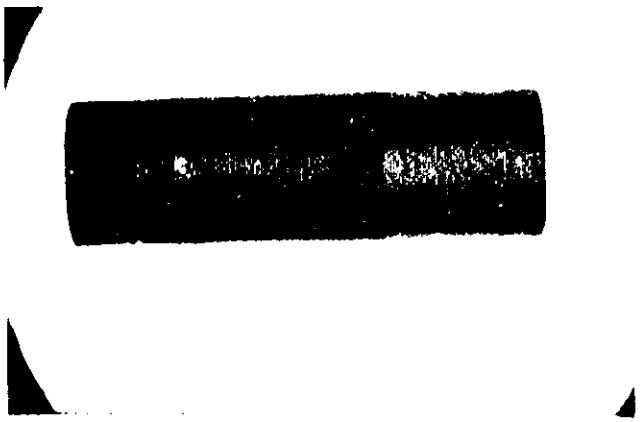

(A) X 2

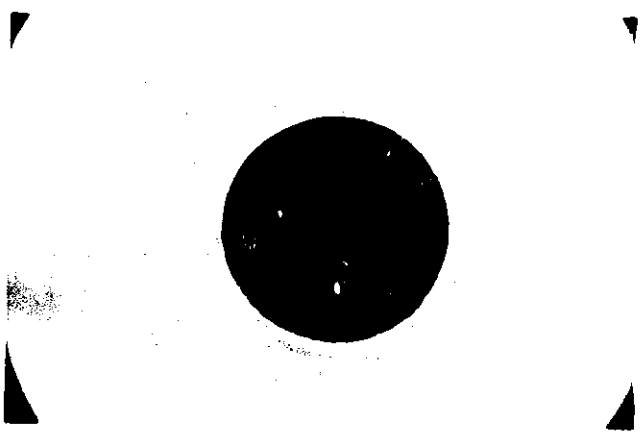

(B) X 3

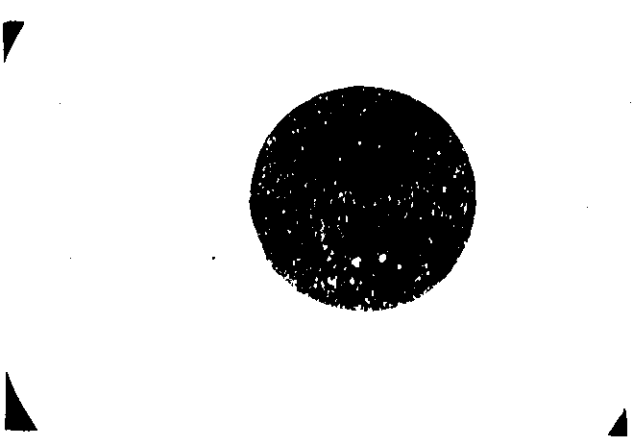

(C) X 3

FIG. 11 SOLID ROD A5

(A) X 2

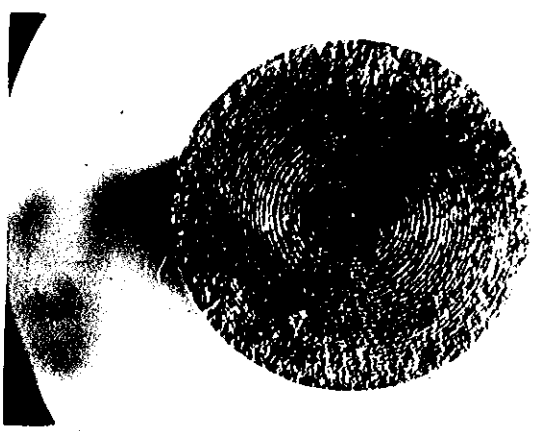

(B) X 3

(C) X 3

FIG. 12 HOLLOW ROD A4

(A) X 2

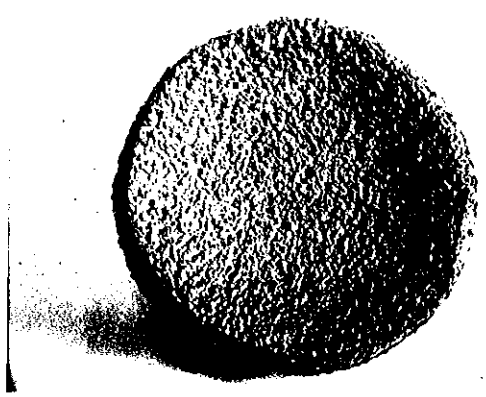

(B) X 3

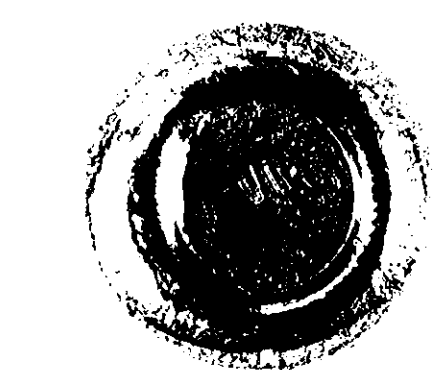

(C) X 3

FIG.13 HOLLOW ROD. A2

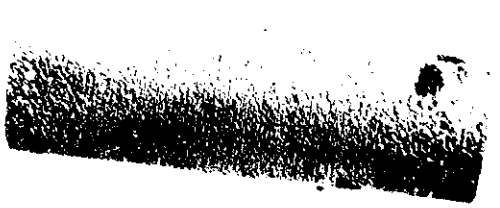

(A) X 2

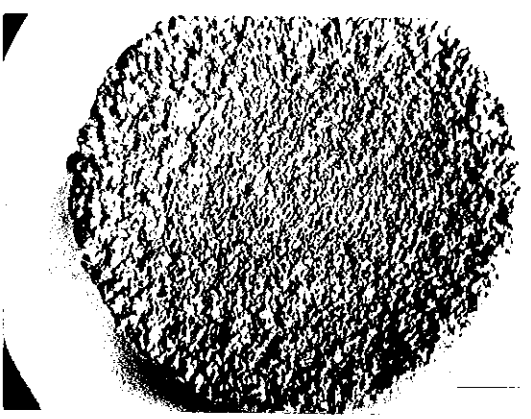

(B) X 6

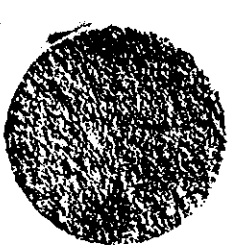

(C) X 3

FIG.14 SOLID ROD. A3

(A) X 2

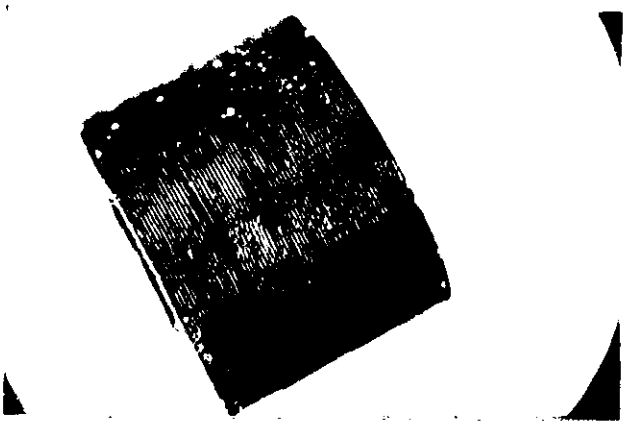

(A) X 3

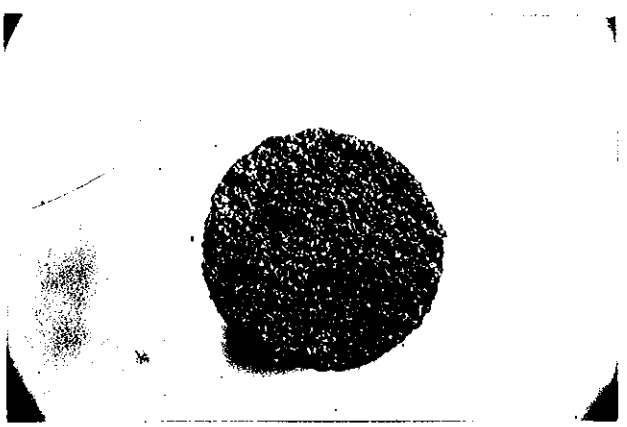

(B) X 3

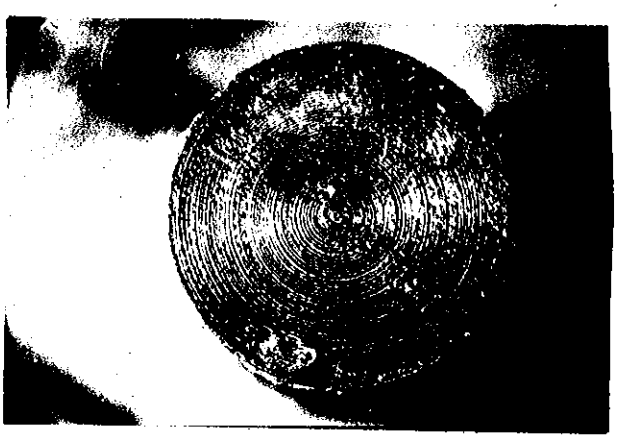

(B) X 3

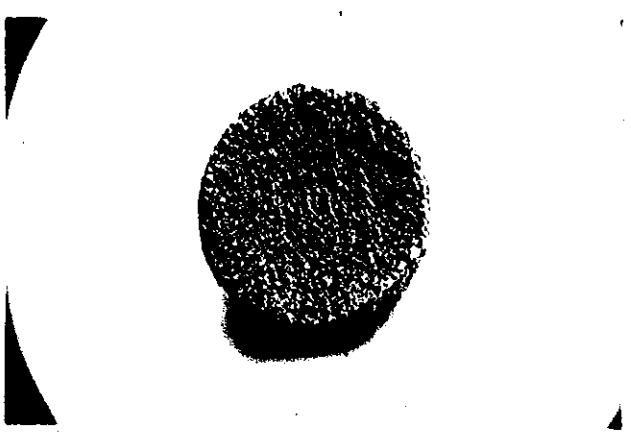

(C) X 3

FIG.15 SOLID ROD B2

(C) X 6

FIG. 16 HOLLOW ROD A8

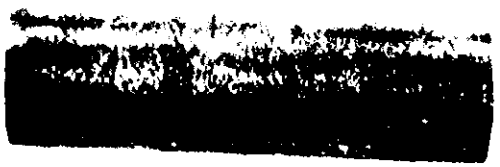

(A) X 2

(A) X 2

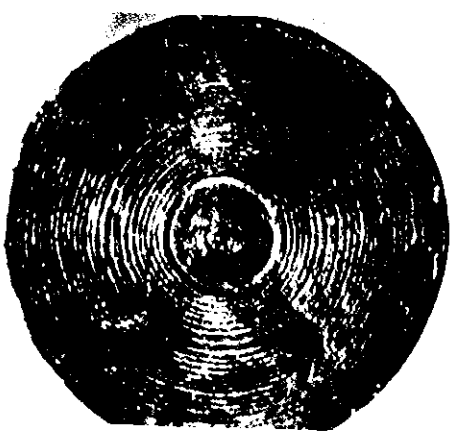

(B) X 6

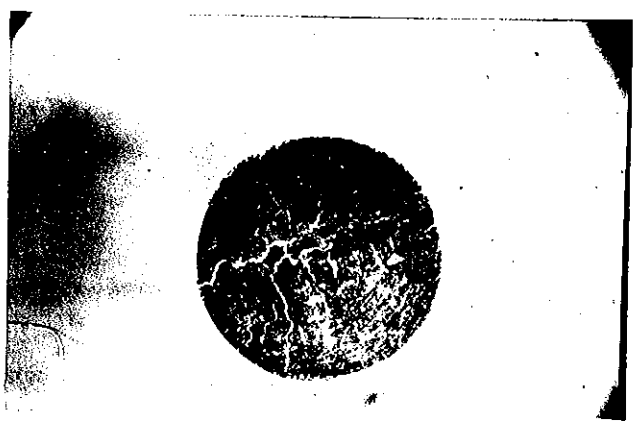

(B) X 2

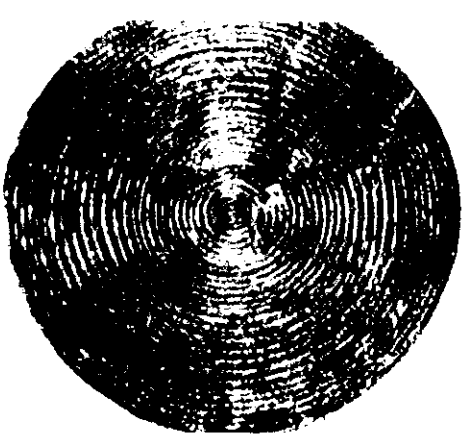

(C) X 6

FIG.17 SOLID ROD B8

(C) X 5

FIG.18 HOLLOW ROD B7

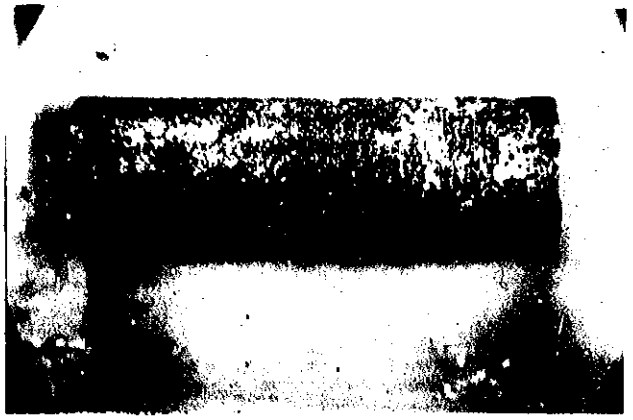

(A) X 2

(A) X 2

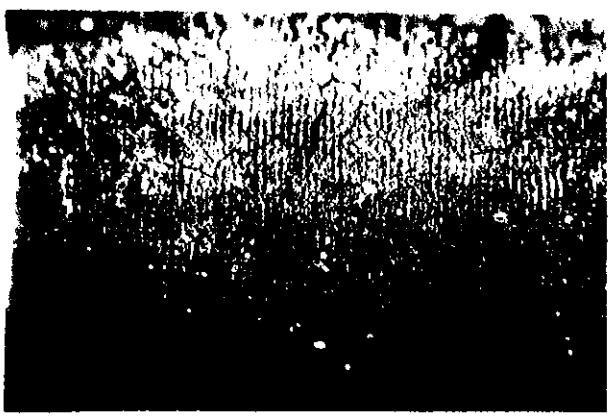

(B) X 6

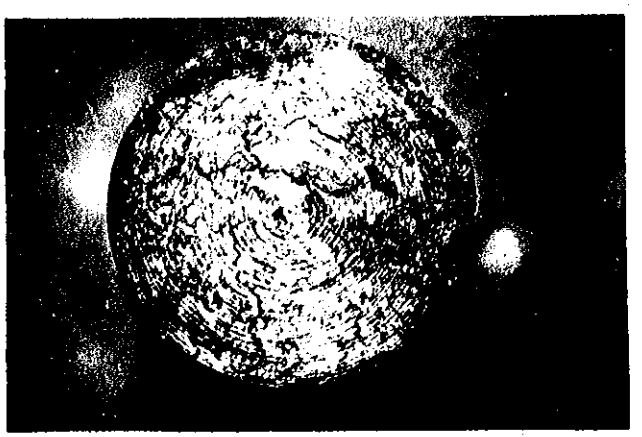

(B) X 3

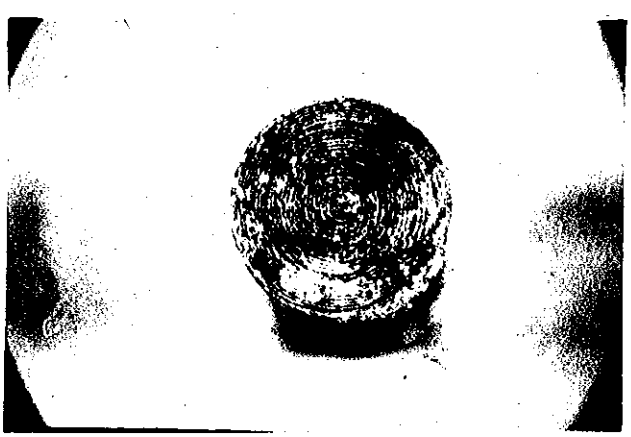

(C) X 3

FIG.19 SOLID ROD B6

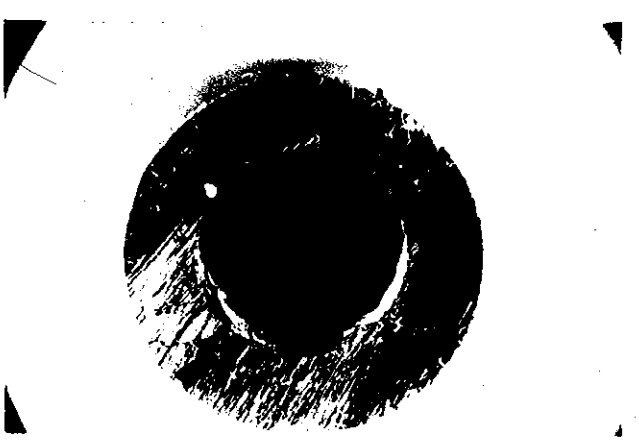

(C) X 3

FIG.20 HOLLOW ROD B5

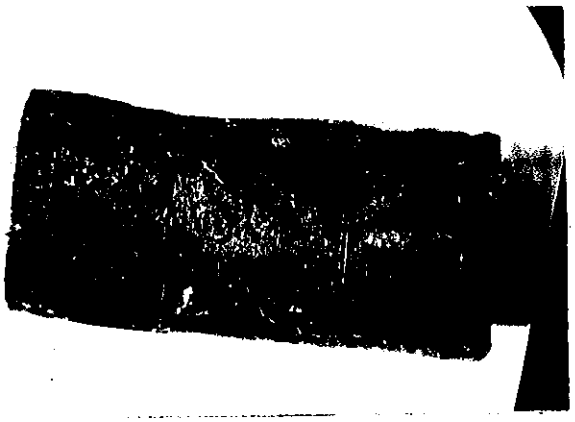

(A) X 2

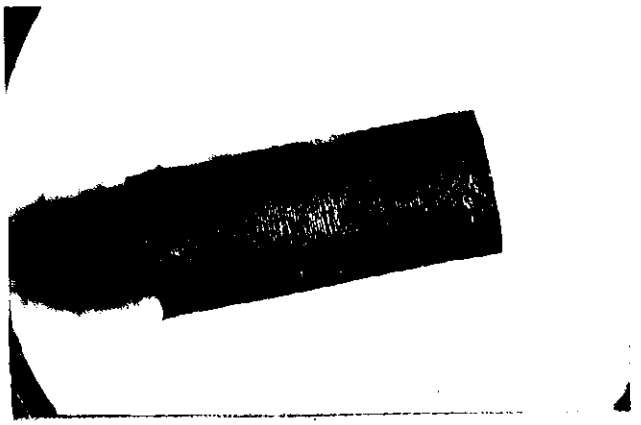

(A) X 2

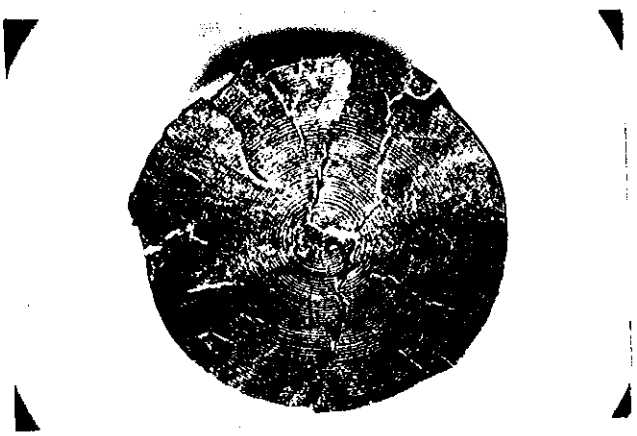

(B) X 3

(B) X 6

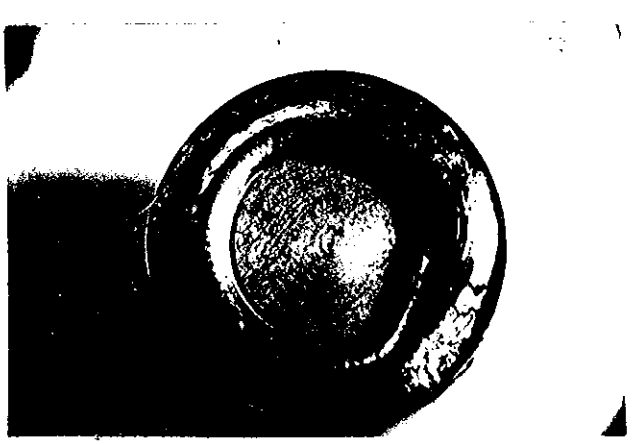

(C) X 3

FIG.21 HOLLOW ROD B3

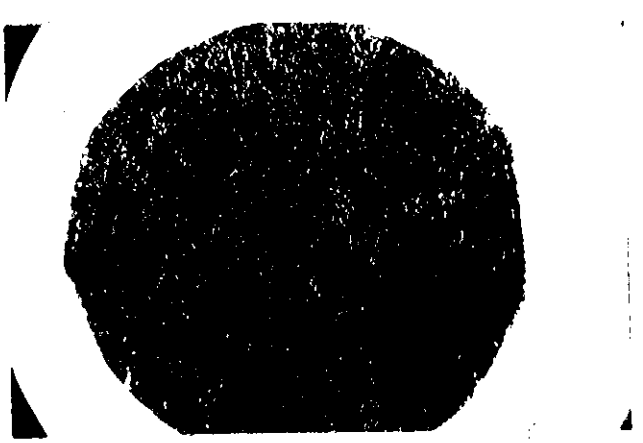

(C) X 6

FIG.22 SOLID ROD B4

Fig. 23
Micrograph of Uranium in the 'as-received' condition

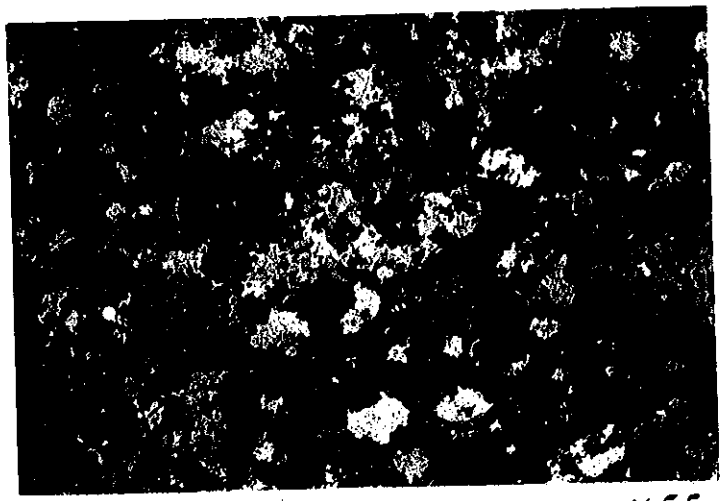

×55

Fig. 24
Micrograph of Control sample for Specimen A-2

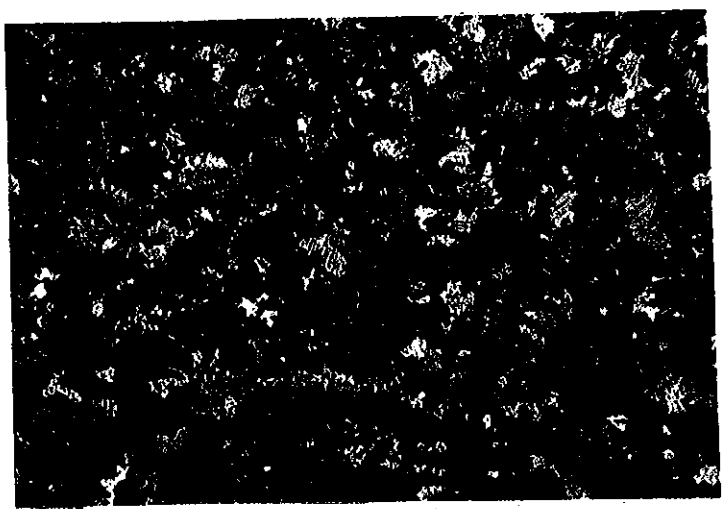

×55

Fig. 25
Micrograph of Control sample for Specimen B-6

×55

a) x42

(b) x42

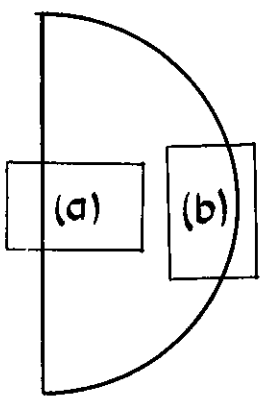

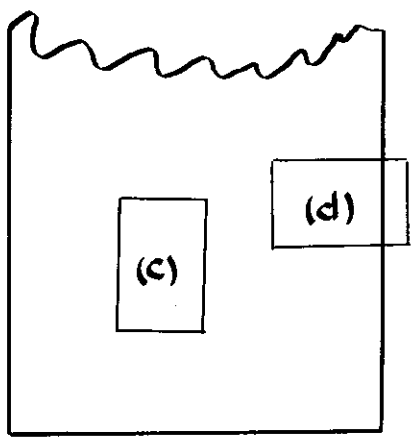

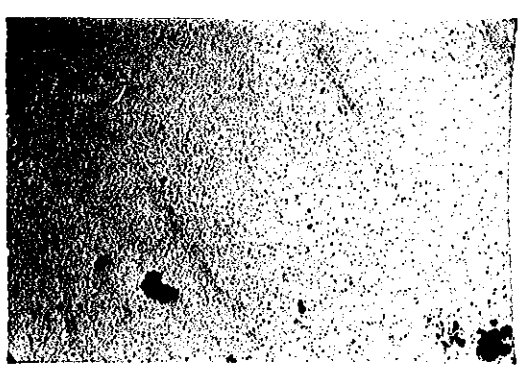

(c) x42

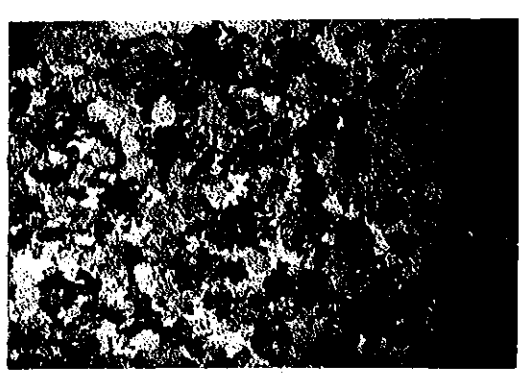

(d) x42

Fig. 26 Micrographs of Specimen A-7
Transverse and Longitudinal Sections

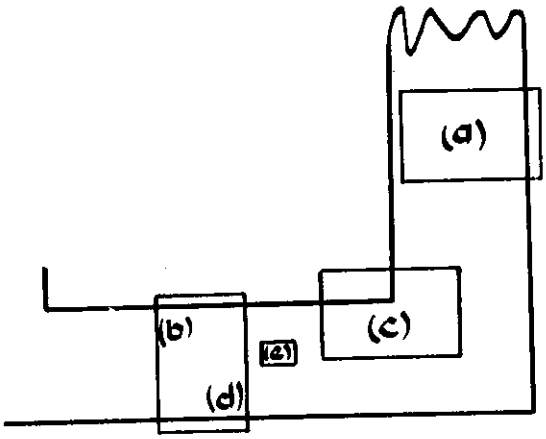

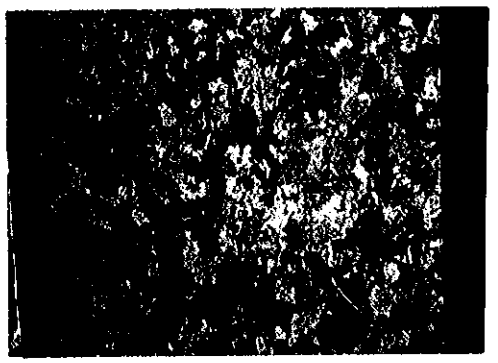

(a) ×42

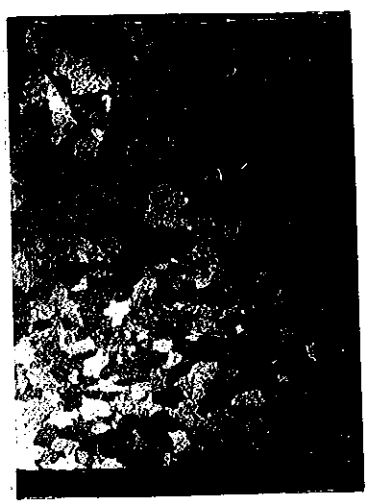

(b) ×42

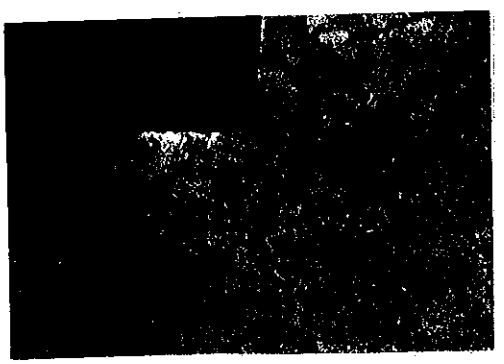

(c) ×42

(d) ×42

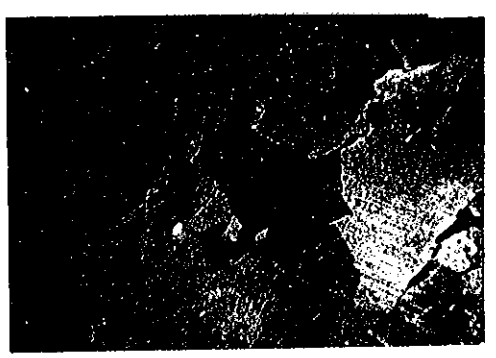

(e) ×150

Fig. 27 Micrographs of Specimen A-6
Longitudinal Section

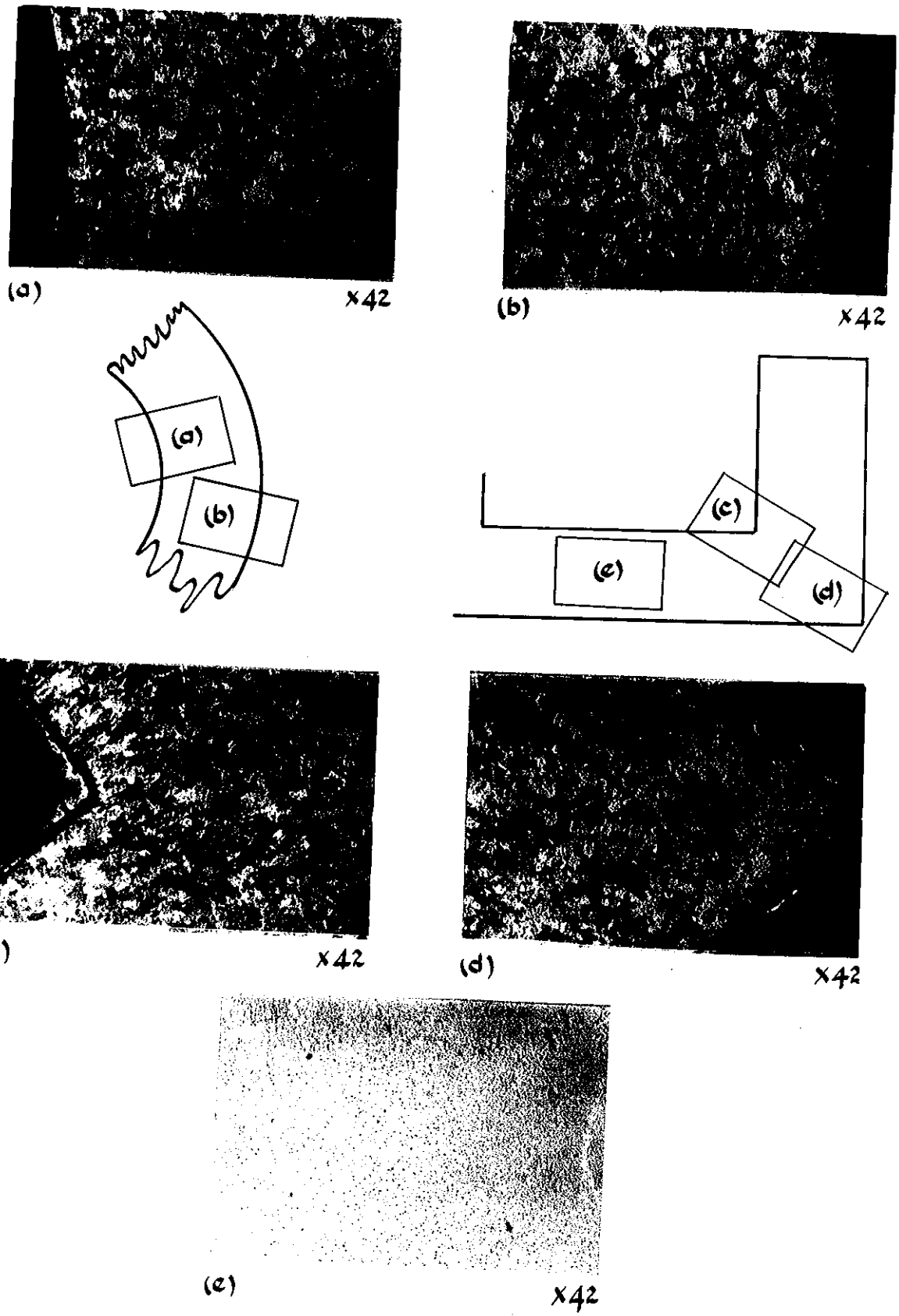

Fig. 28 Micrographs of Specimen A-4.
Transverse and Longitudinal Sections

(a) x42

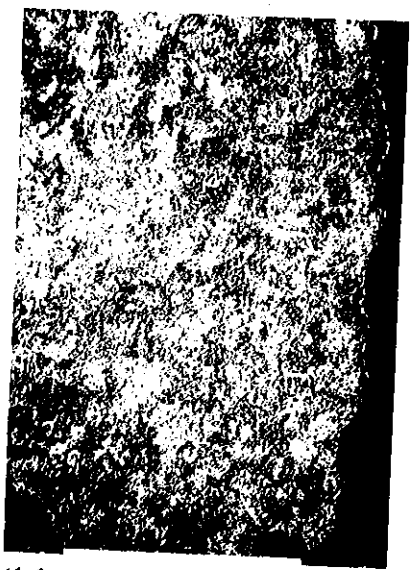

(b) x42

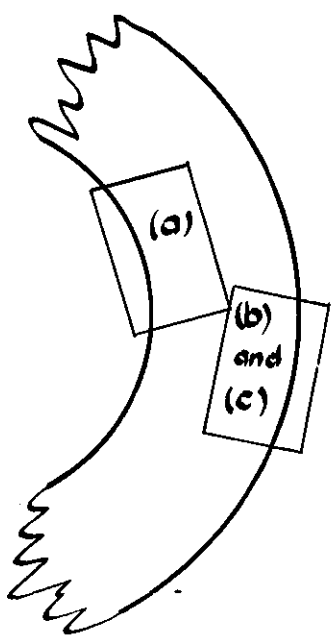

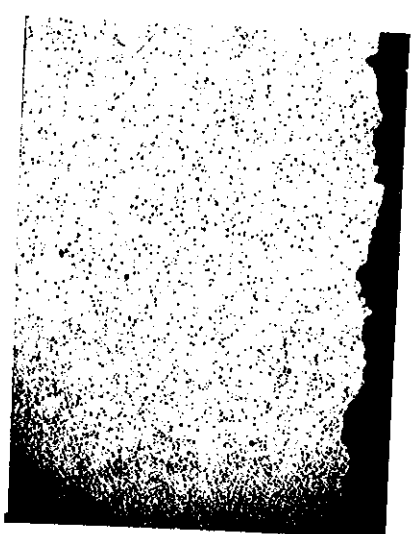

(c) x42

Fig. 29 Micrographs of Specimen A-2 Transverse Section

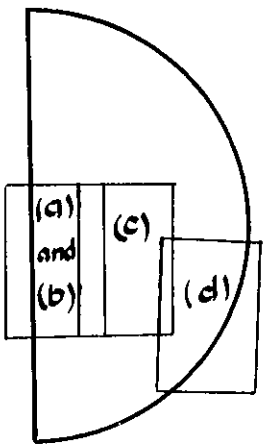

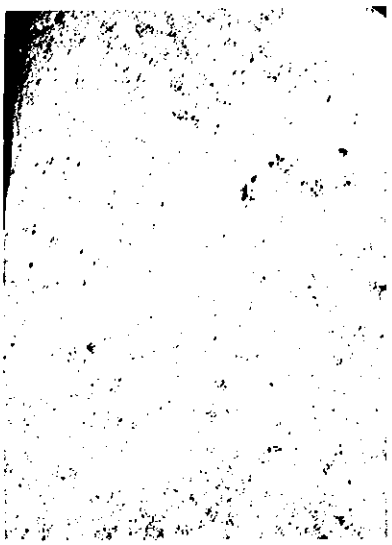

(a) ×42

(b) ×42

(c) ×42

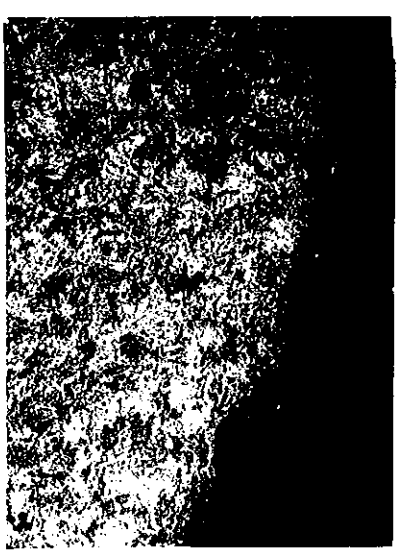

(d) ×42

Fig. 30 Micrographs of Specimen B-2
Transverse Section

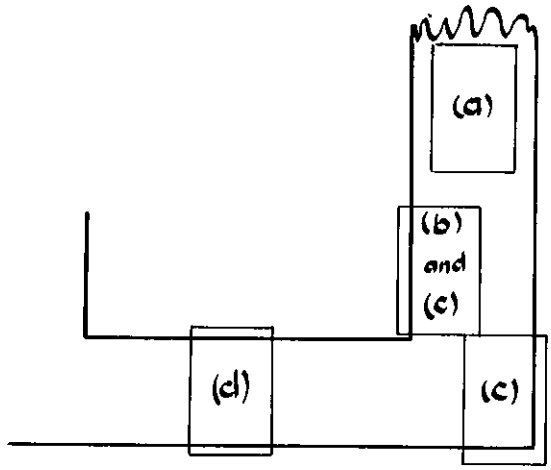


(a) x42

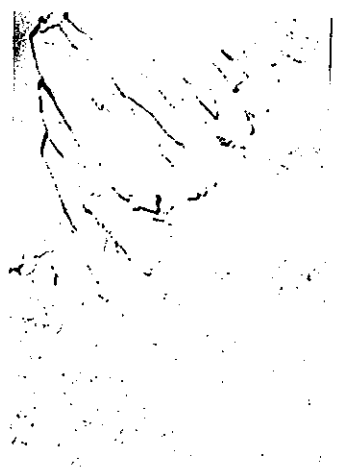
(b) x42


(c) x42


(d) x42


(e) x42

Fig 31 Micrographs of Specimen A-8
Longitudinal Section

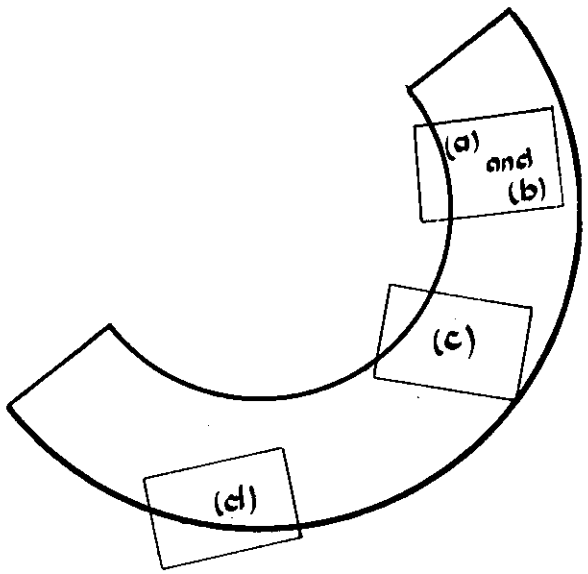

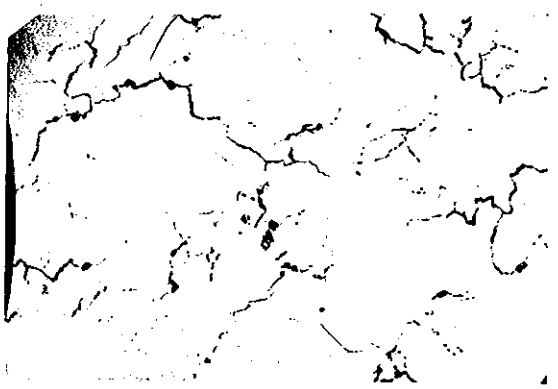

(a) x42

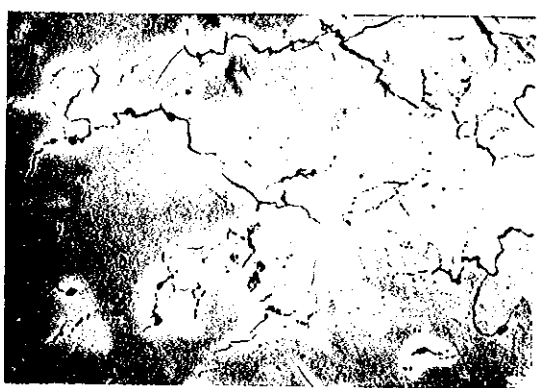

(b) x42

Tarnished surface showing haloes around hydride particles

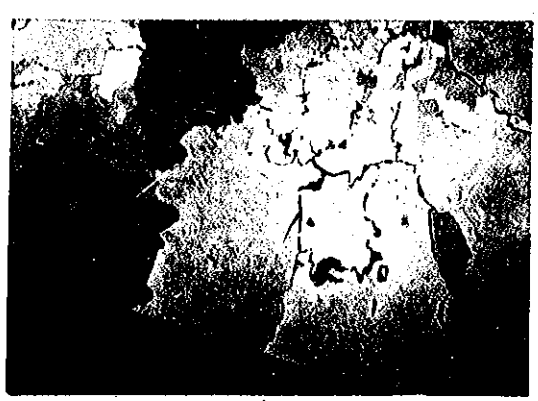

(d) x42

Note :- displacement at surface associated with grain boundary ~~~~

(c) x42

Fig. 32 Micrographs of Specimen A-8 Transverse Section through Upper End

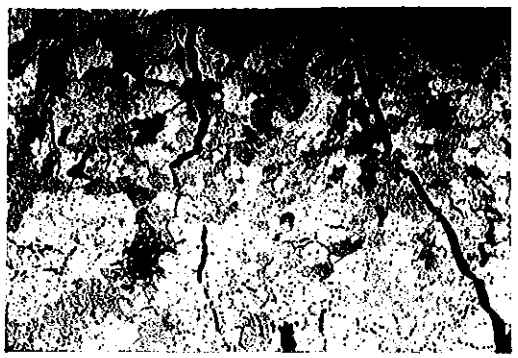

(a) ×42

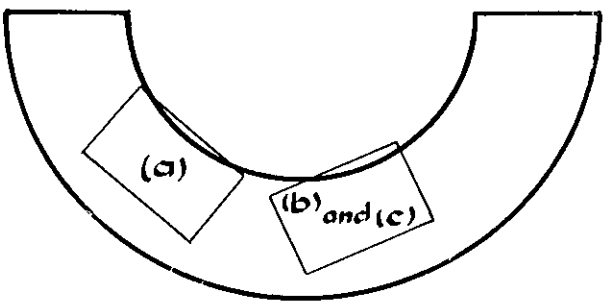

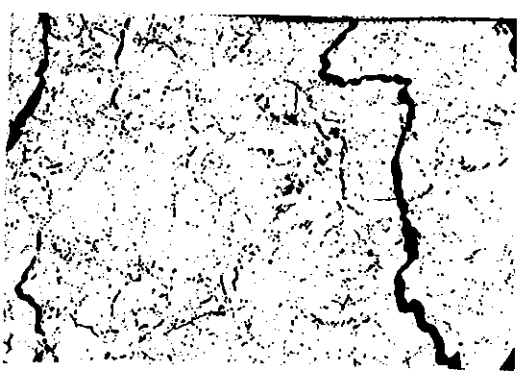

(b) ×42

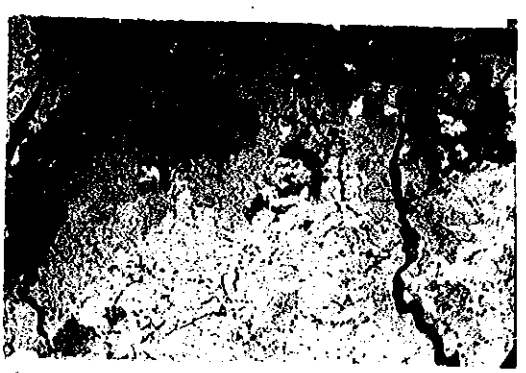

(c) ×42

Fig. 33 Micrographs of Specimen B-7
Transverse Section of Upper End

(a) ×42

(b) ×42

(c) ×42

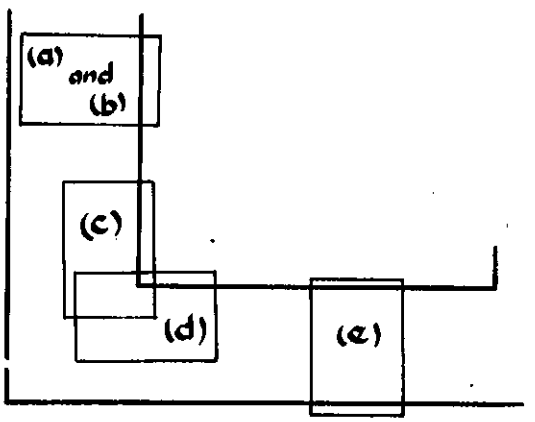

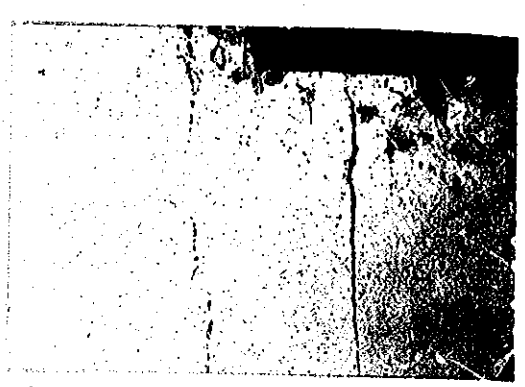

(d) ×42

(e) ×42

Fig. 34 Micrographs of Specimen B-7 Longitudinal Section

(a) x42

(b) x42

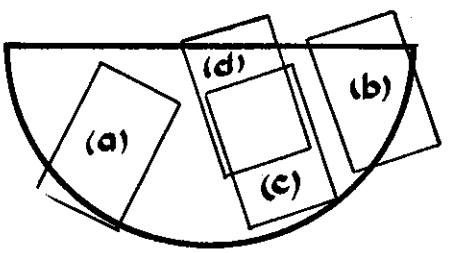

(c) x42

(d) x42

Fig 35 Micrographs of Specimen B-6
Transverse Section

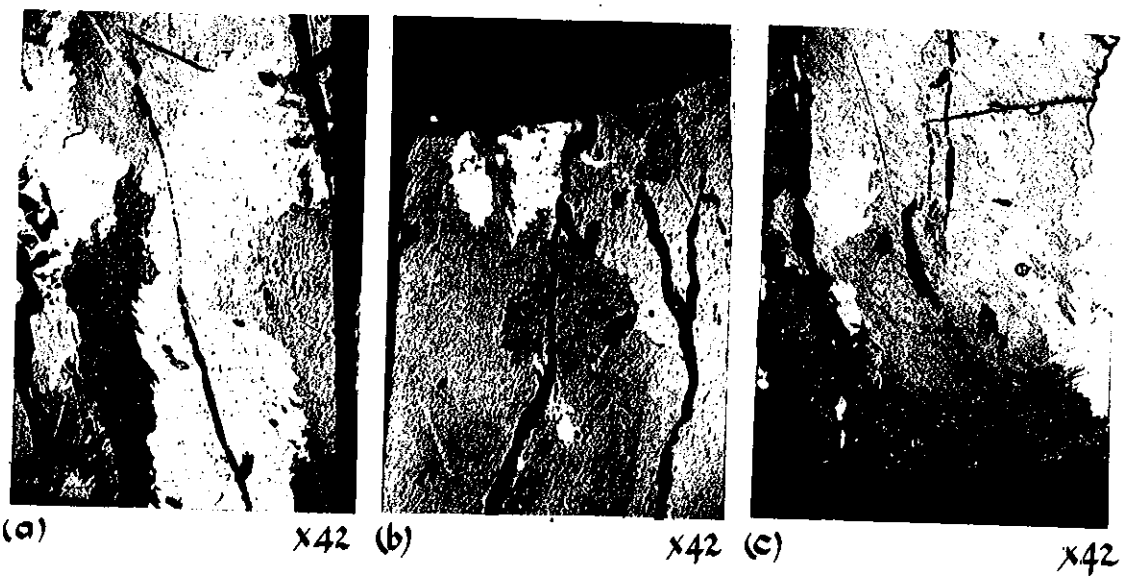

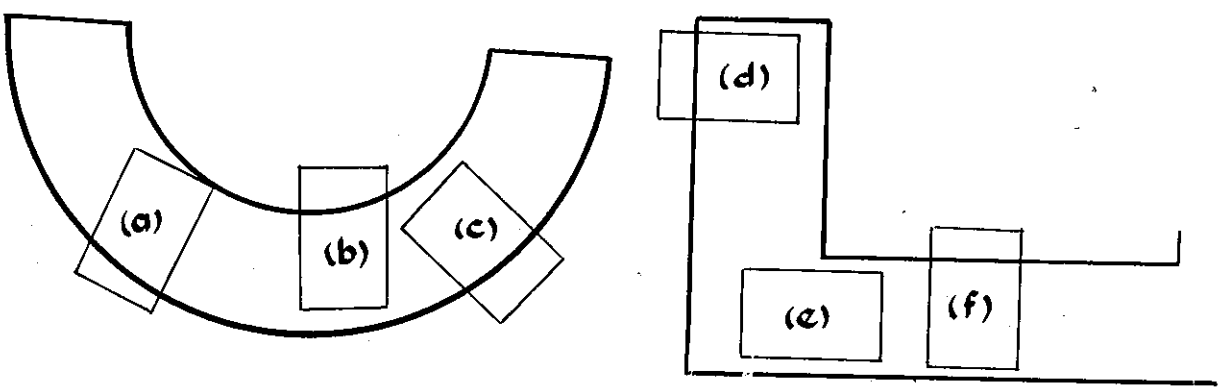

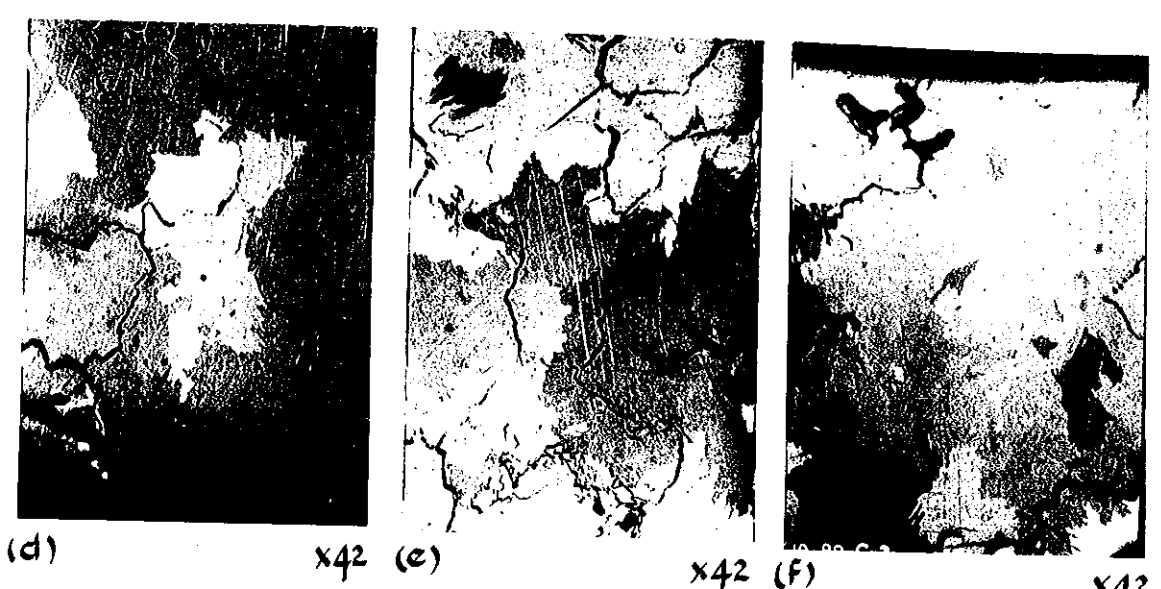

Fig.36 Micrographs of Specimen B-5
Transverse and Longitudinal Sections

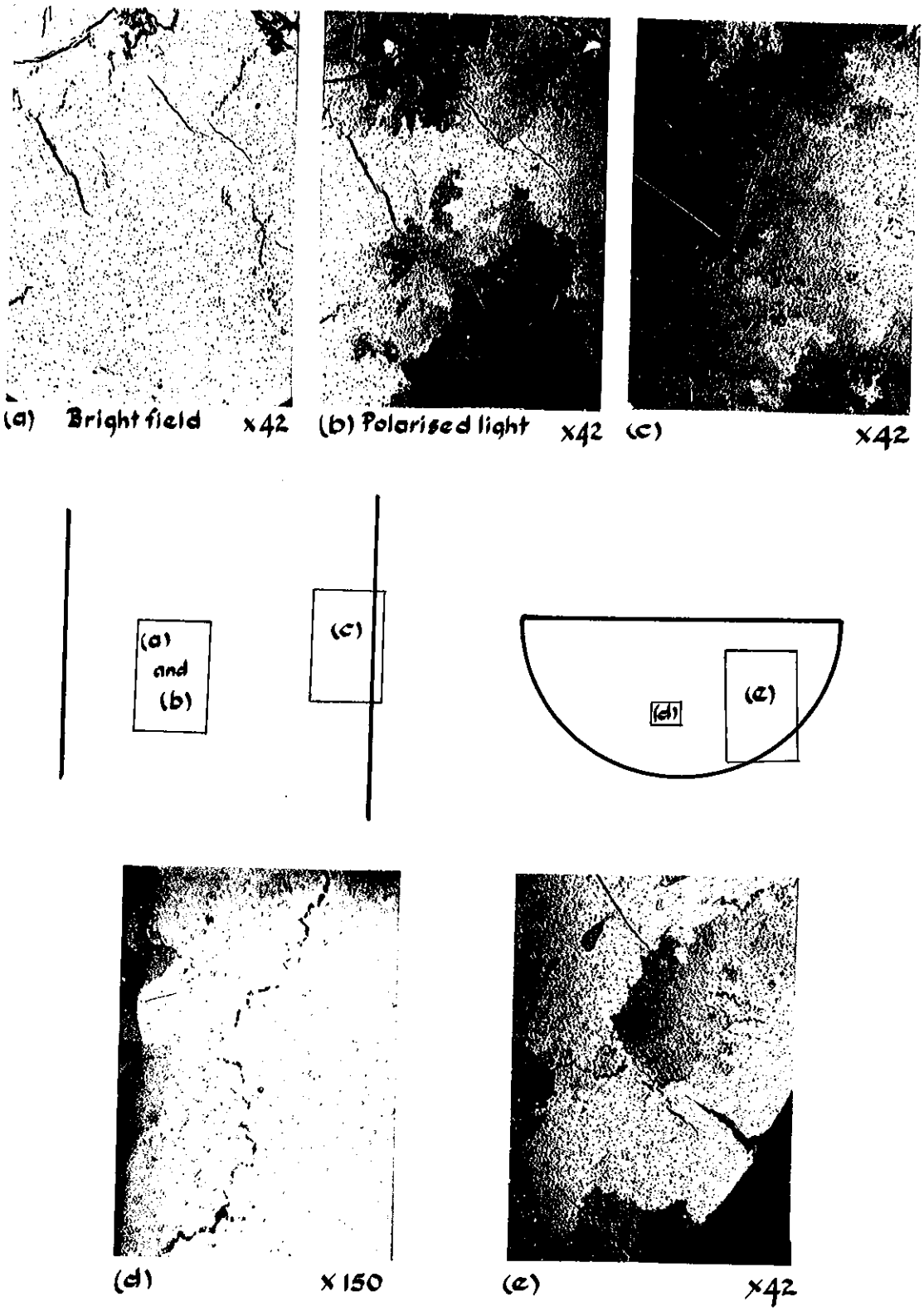

Fig. 37 Micrographs of Specimen B-8
Longitudinal and Transverse Sections

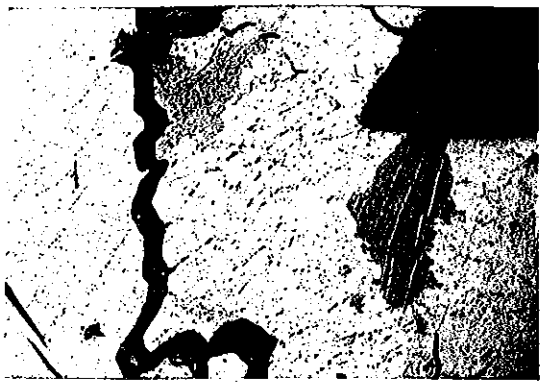

(a) x42

(b) x42

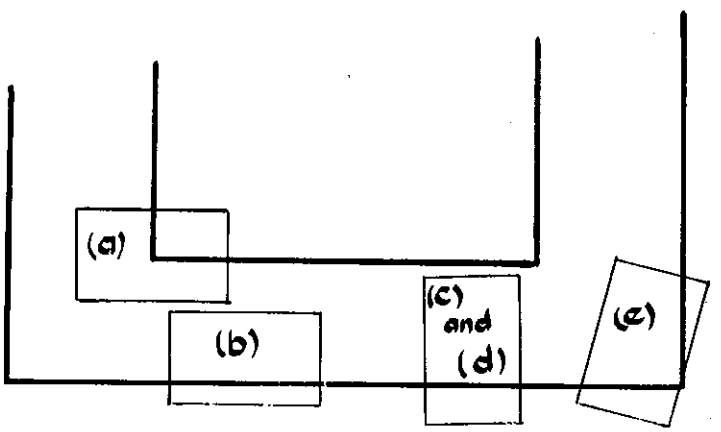

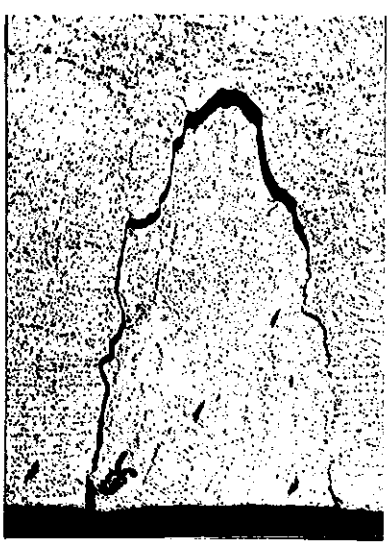

(c) Bright field x42

(d) Polarised light x42

(e) x42

Fig. 38 Micrographs of Specimen B-3
Longitudinal Section

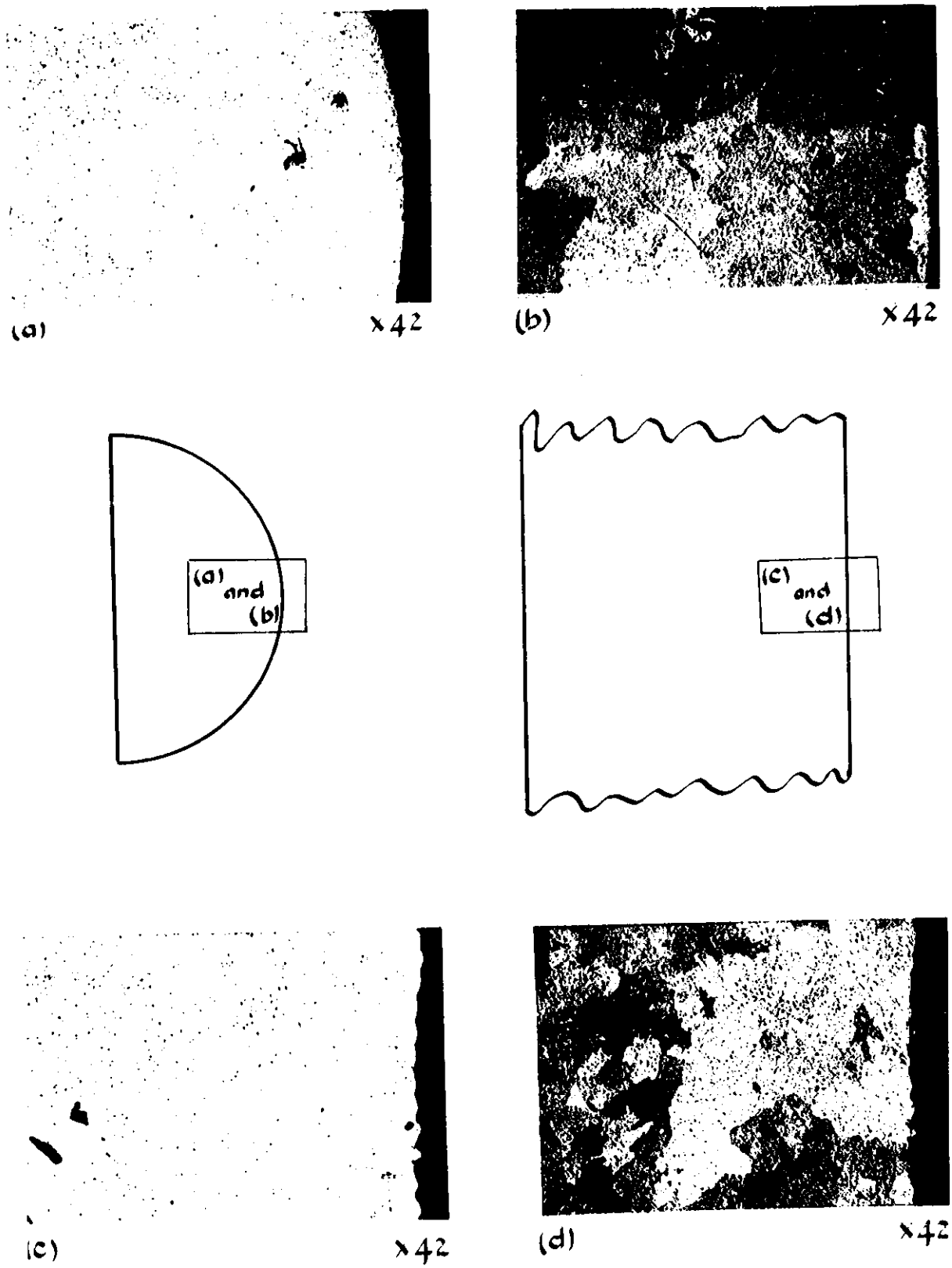

Fig. 39 Micrographs of Specimen B-4.
Transverse and Longitudinal Sections

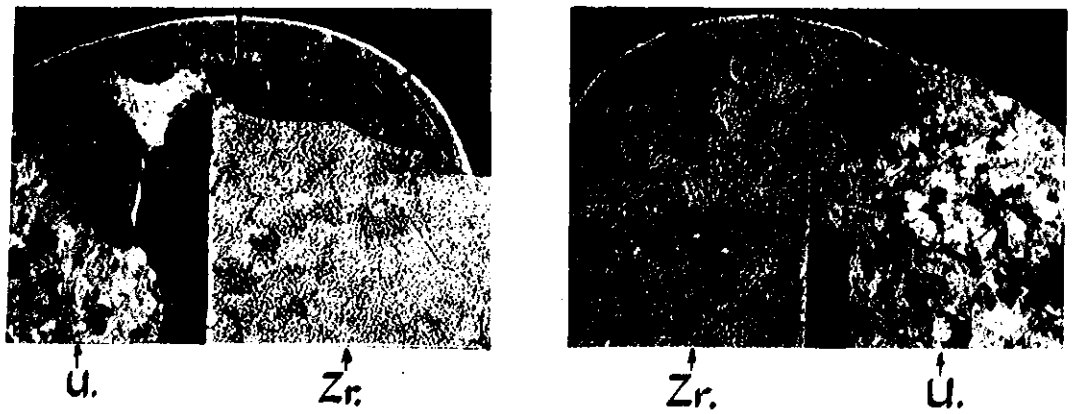

Fig.40 Specimen A-6

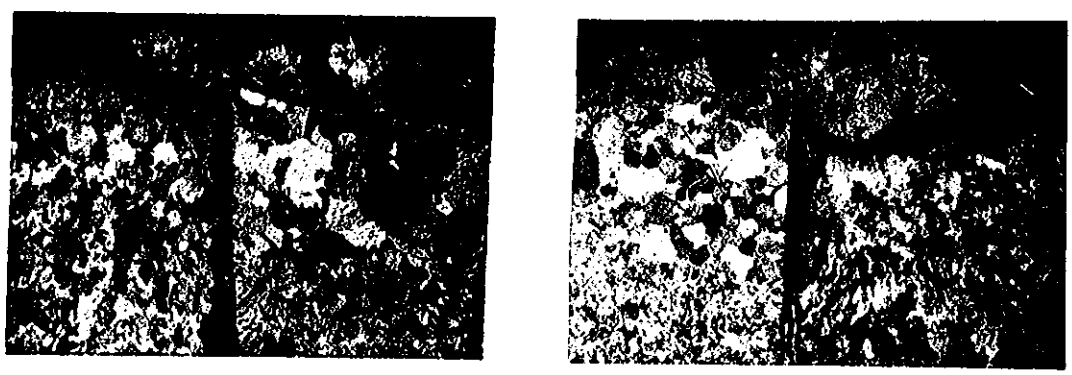

Fig.41 Specimen A-4

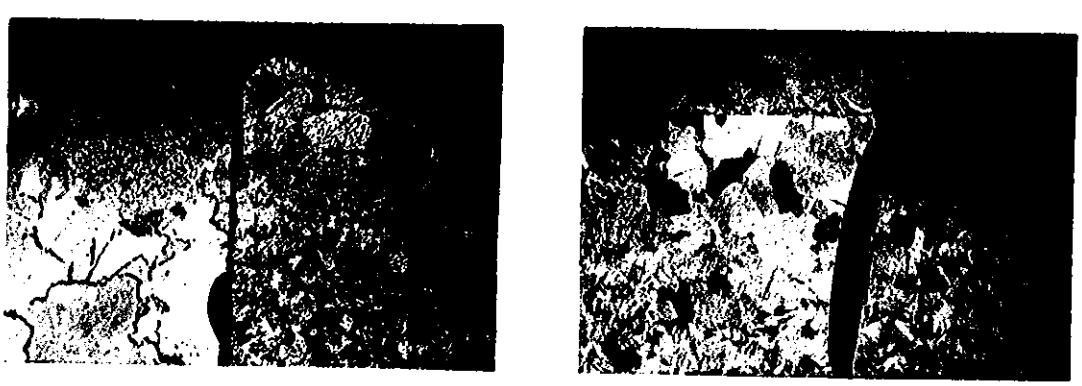

Fig.42 Specimen A-8

Micrographs of Longitudinal Section through the welds in Specimens A6, A4 and A8. The Zirconium is on the inside in each case ~ ~ ~ ~

X42

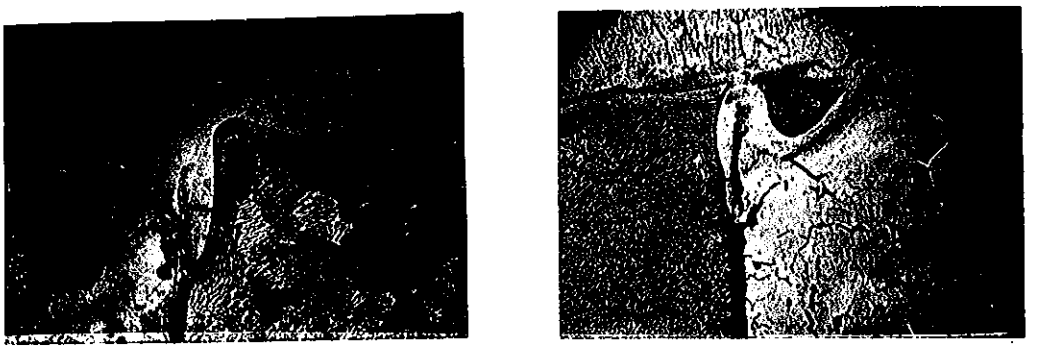

U. Zr. Zr. U.

Fig.43 Specimen B-7

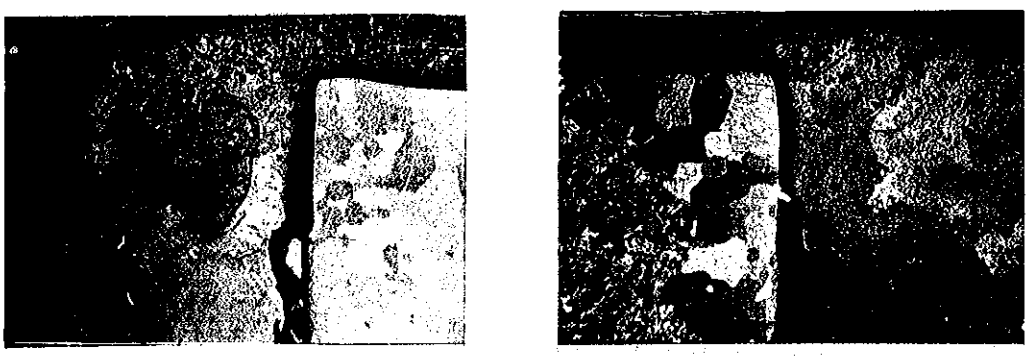

Fig.44 Specimen B-5

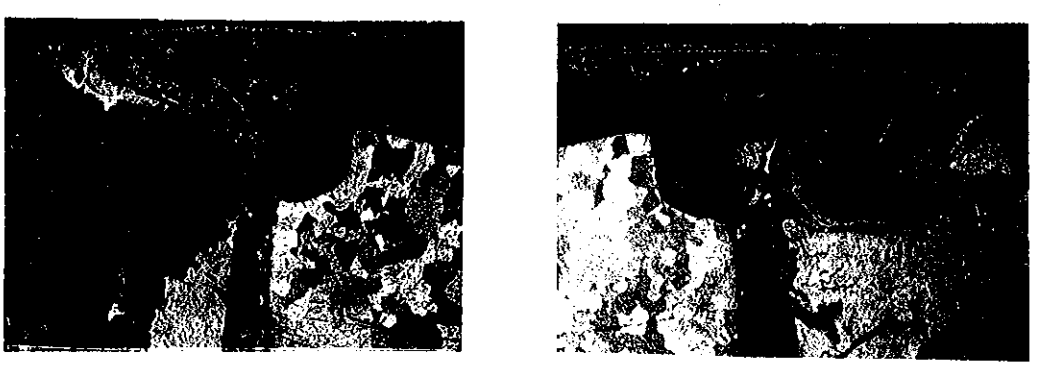

Fig.45 Specimen B-3

Micrographs of Longitudinal Section through the welds in Specimens B7, B5 and B3. The Zirconium is on the inside in each case. ~ ~ ~ ~

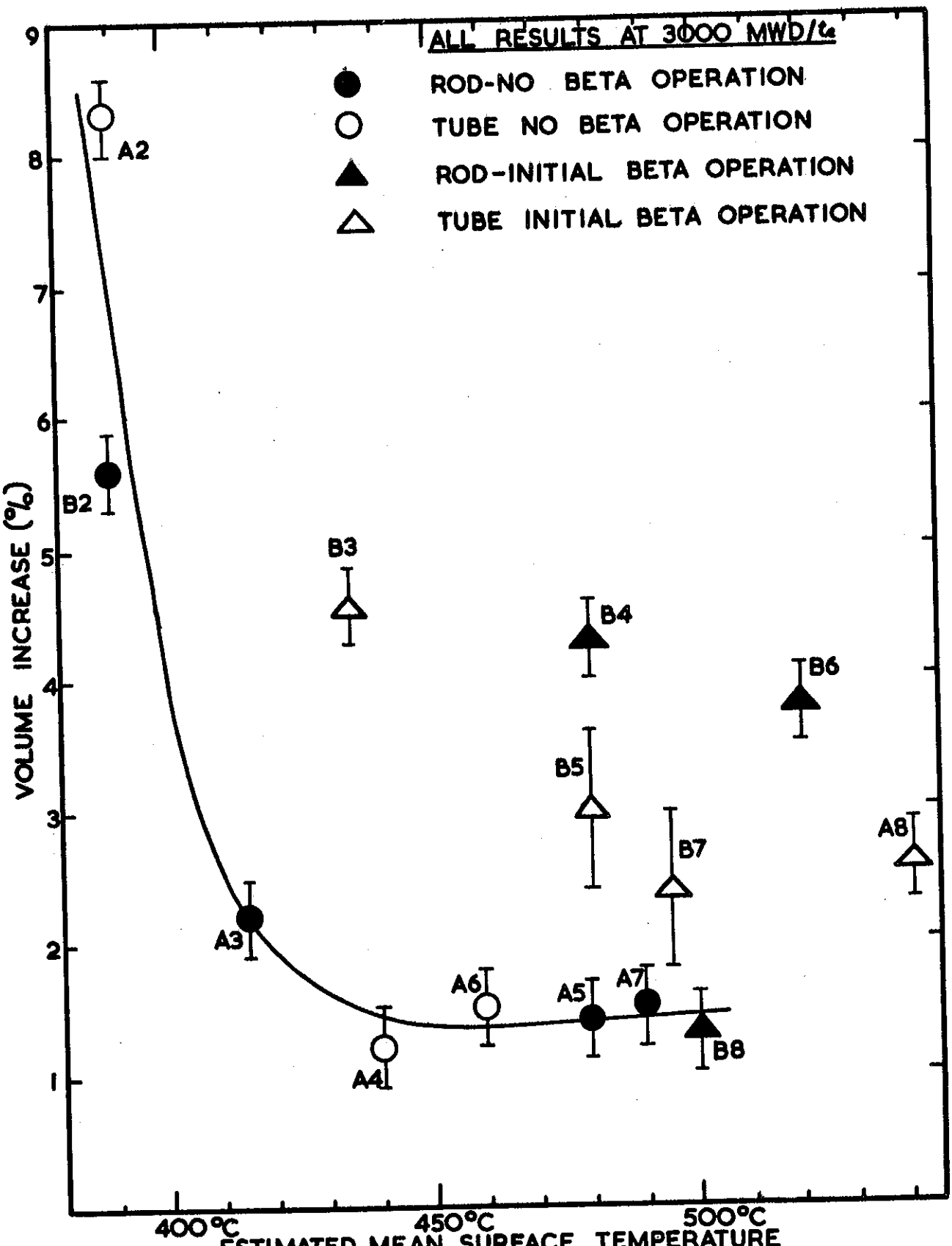

FIG. 46 VOLUME INCREASE AT 3000 MWD/te vs. ESTIMATED MEAN SURFACE TEMPERATURE

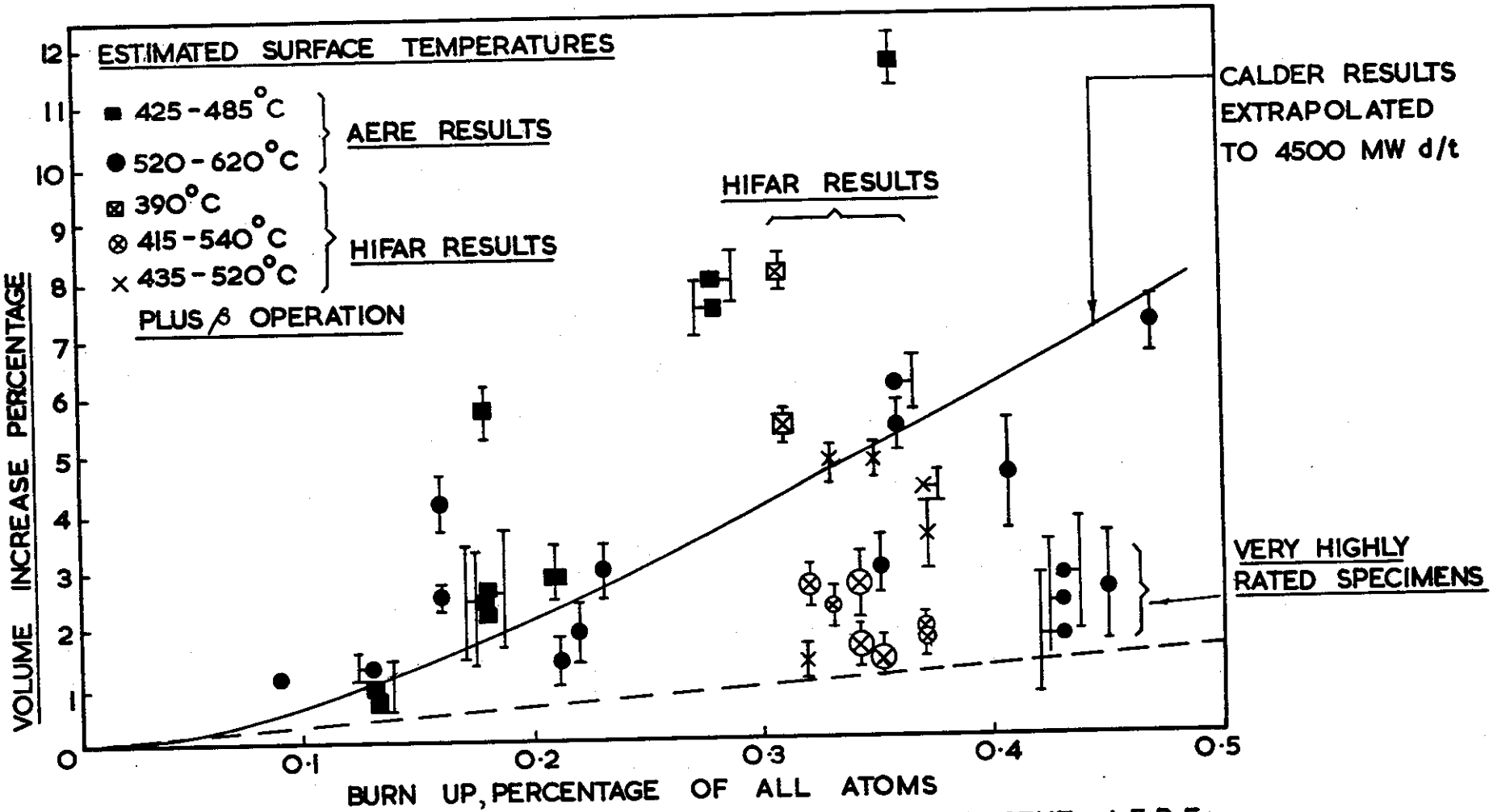

FIGURE 47 COMPARISON OF THE PRESENT RESULTS WITH RECENT A.E.R.E. RESULTS QUOTED BY PUGH, SHOWING BURN UP/ VOLUME INCREASE RELATIONSHIP

DISTRIBUTION

A.A.E.C.

Standard (24)	Dr. K.D. Reeve	Mr. G.A. Tingate
Dr. R. Smith	Mr. F.L. Bett	Mr. M.S. Farrell
Mr. B.S. Hickman	Mr. D.R. Ebeling	Mr. R.N. Whittem
Mr. R.J. Hilditch	Mr. W.J. Turner	Mr. G.L. Hanna
Mr. W.J. Wright		

UNITED KINGDOM

Standard (R.F.L. Springfields)		Dr. J.F.W. Bishop	S
Mr. J. Harper	S	Dr. G.B. Greenough	S
Mr. D.O. Pickman	S	Mr. J.K. O'Sullivan	S
File	R.S.		
Libraries 6.2.2.2.2.2.	R.S.C.W.D.Ca		
2.2.2.12.3.	CC. H. WH. T.N.P.G. E.E. Co		
1.3.3.4.	B&W GEC/SC APC CEGB		
Spares 10	S		

N.P.C.C.–F.E.W.P. (Unless above)

Mr. R.A. Shaw	S	Dr. A.T. Churchman	C.E.G.B.
Mr. D.H. Willey	S	Mr. E.H. Parfrey	C.E.G.B.
Mr. E.C.W. Perryman	C	Mr. J. Henderson (2)	S.S.E.B.
Dr. P.E. Brookes	C	Mr. R.A. Skinner	T.N.P.G.
Mr. T. Edge	R	Mr. G.M. Emsley	"
Mr. N. McLaren	R	Mr. J.W. Hughes	"
Mr. V. Walker	W	Dr. G.W. Ardley	A.P.P. (E.E.(0).
Dr. V.W. Eldred	W	Mr. A.J. Williams	" "
Mr. B.W. Mott	H	Dr. B.C. Woodfine	G.E.C./S.C.
Dr. A. Moore	A	Dr. M.W. Davies	G.E.C./S.C.
Mr. G.C. Ellis	A	Mr. W.G. Hull	A.P.C.
		Mr. P.C. Warner	A.P.C.

Additional (Rapporteurs) (unless above)

Dr. F.S. Martin	S	Mr. L.R. Williams	S	Mr. J.M. Hartog	S
Mr. A.E. Williams	S	Dr. R.W.M. D'Eye	S	Mr. P.B.F. Evans	Ca
Mr. J.H. Gittus	S	Mr. W.T. Edwards	C	Mr. J. Pendleton	R

N.P.C.C. (unless above)

Sir William Cook	London Office

Additional

Mr. L. Grainger	H

Tokai–Mura T.R.C.W.P.

Mr. H. Cullen	R	Mr. C.S. Campbell	C	Mr. D.W. Bottle	G.E.C.	Erith
Dr. N. Davis	R	Mr. C. Boorman	Ca	Mr. P. Hawkes	"	"
Mr. K.H. Dent	R	Mr. D.W. Harris	S	Dr. W.L. Mercer	"	"
Mr. N.H. McLaren	R	Mr. I.H. Morrison	S	Mr. A.R. Pickering	"	"
Mr. T.A. Seeley (Sec.)	R					

Additional

Mr. F. Butler	R	Mr. R.V. Moore	R	Mr. H. Rose	D	Dr. R.G. Skipper	G.E.C.
Mr. H. Cartwright	R	Mr. K.A. Sanson	S	Mr. E. Proudfoot	C	Dr. P. Murray	H
Mr. J.B.W. Cunningham	R	Mr. R. Baggot	S	Mr. E. Davies	S	Mr. S.F. Pugh	H
Mr. C.L. Dodd	R	Dr. E. Hyam	W	Mr. H.E. Dibben	S	Mr. O.S. Plail	H
Mr. T.J. Heal	R	Mr. D. Shaw	W	Mr. I.P. Jones	S	Mr. R.G. Bellamy	H
Mr. G.H. Inglis	R	Mr. J. Skinner	W	Mr. J.J. Stubbs	R	Mr. L.M. Wyatt	C.E.G.B.
Mr. J. Tatlock	R	Dr. S. Cottrell	D	Mr. P.R. Dixon	G.E.C.	Mr. J.C. Bell	S